New Constraints on $\Omega_{\rm M}$, Ω_Λ, and w from an Independent Set of Eleven High-Redshift Supernovae Observed with HST[1]

SUBMISSION CANDIDATE 3

R. A. Knop[2,3,4], G. Aldering[5,4], R. Amanullah[6], P. Astier[7], K. Barton[8], G. Blanc[5,7], M. S. Burns[8], A. Conley[5,9], S. E. Deustua[5,10], M. Doi[11], R. Ellis[12], S. Fabbro[13,4], G. Folatelli[6], A. S. Fruchter[14], G. Garavini[6], S. Garmond[5,9], R. Gibbons[5], G. Goldhaber[5,9], A. Goobar[6], D. E. Groom[5,4], D. Hardin[7], I. Hook[15], D. A. Howell[5], M. Irwin[16], A. G. Kim[5,4], B. C. Lee[5], C. Lidman[17], R. McMahon[16], J. Mendez[18,19], S. Nobili[6], P. E. Nugent[5,4], R. Pain[7], N. Panagia[14], C. R. Pennypacker[5], S. Perlmutter[5], R. Quimby[5], J. Raux[7], N. Regnault[5,23], P. Ruiz-Lapuente[19], G. Sainton[7], B. Schaefer[20], K. Schahmaneche[7], E. Smith[2], A. L. Spadafora[5], V. Stanishev[6], M. Sullivan[21,12], N. A. Walton[16], L. Wang[5], W. M. Wood-Vasey[5,9], and N. Yasuda[22]
(THE SUPERNOVA COSMOLOGY PROJECT)

ABSTRACT

This paper presents measurements of $\Omega_{\rm M}$, Ω_Λ, and w from eleven supernovae at $z = 0.36$–0.86 with high-quality lightcurves measured using WFPC2 on the HST. This is an independent set of high-redshift supernovae that confirms previous supernova evidence for an accelerating Universe. The high-quality lightcurves available from photometry on WFPC2 mean that these eleven supernovae alone provide measurements of the cosmological parameters comparable in statistical weight to the previous results. Combined with earlier Supernova Cosmology Project data, the new supernovae yield a measurement of the mass density $\Omega_{\rm M} = 0.22 \pm 0.06$ (statistical) ± 0.04 (identified systematics), or equivalently, a cosmological constant of $\Omega_\Lambda = 0.78 \pm 0.06$ (statistical) ± 0.04 (identified systematics), under the assumptions of a flat universe and that the dark energy equation of state parameter has a constant value $w = -1$. When the supernova results are combined with independent flat-universe measurements of $\Omega_{\rm M}$ from CMB and galaxy redshift distortion data, they provide a measurement of $w = -1.06^{+0.14}_{-0.21}$ (statistical) ± 0.08 (identified systematic), if w is assumed to be constant in time. In addition to high-precision lightcurve measurements, the new data offer greatly improved color measurements of the high-redshift supernovae, and hence host-galaxy extinction estimates; there is no trend of anomalous $E(B\text{-}V)$ at higher redshifts. The precision of the measurements is such that it is possible to perform a host-galaxy extinction correction directly to individual supernovae without any assumptions or priors on the parent $E(B\text{-}V)$ distribution, yielding cosmological results consistent with current and previous results, and still requiring dark energy with probability $P > 0.99$.

[1]Based in part on observations made with the NASA/ESA Hubble Space Telescope, obtained at the Space Telescope Science Institute, which is operated by the Association of Universities for Research in Astronomy, Inc., under NASA contract NAS 5-26555. These observations are associated with programs GO-7336, GO-7590, and GO-8346. Some of the data presented herein were obtained at the W.M. Keck Observatory, which is operated as a scientific partnership among the California Institute of Technology, the University of California and the National Aeronautics and Space Administration. The Observatory was made possible by the generous financial support of the

W.M. Keck Foundation. Based in part on observations obtained at the WIYN Observatory, which is a joint facility of the University of Wisconsin-Madison, Indiana University, Yale University, and the National Optical Astronomy Observatory. Based in part on observations made with the European Southern Observatory telescopes (ESO programmes 60.A-0586 and 265.A-5721) Based in part on observations made with the Canada-France-Hawaii Telescope, operated by the National Research Council of Canada, le Centre National de la Recherche Scientifique de France, and the University of Hawaii.

[2]Department of Physics and Astronomy, Vanderbilt University, Nashville, TN 37240, USA

[3]Visiting Astronomer, Kitt Peak National Observatory, National Optical Astronomy Observatory, which is operated by the Association of Universities for Research in Astronomy, Inc. (AURA) under cooperative agreement with the National Science Foundation.

[4]Visiting Astronomer, Cerro Tololo Interamerican Observatory, National Optical Astronomy Observatory, which is operated by the Association of Universities for Research in Astronomy, Inc. (AURA) under cooperative agreement with the National Science Foundation.

[5]E. O. Lawrence Berkeley National Laboratory, 1 Cyclotron Rd., Berkeley, CA 94720, USA

[6]Department of Physics, Stockholm University, SCFAB, S-106 91 Stockholm, Sweden

[7]LPNHE, CNRS-IN2P3, University of Paris VI & VII, Paris, France

[8]Colorado College 14 East Cache La Poudre St., Colorado Springs, CO 80903

[9]Department of Physics, University of California Berkeley, Berkeley, 94720-7300 CA, USA

[10]American Astronomical Society, 2000 Florida Ave, NW, Suite 400, Washington, DC, 20009 USA.

[11]Department of Astronomy and Research Center for the Early Universe, School of Science, University of Tokyo, Tokyo 113-0033, Japan

[12]California Institute of Technology, E. California Blvd, Pasadena, CA 91125, USA

[13]Centro, Multidisiplinar de Astrofísica, Instituo, Superior Técnico, Lisbo

[14]Space Telescope Science Institute, 3700 San Martin Drive, Baltimore, MD 21218, USA

[15]Department of Physics, University of Oxford, Nuclear & Astrophysics Laboratory Keble Road, Oxford, OX1 3RH, UK

[16]Institute of Astronomy, Madingley Road, Cambridge CB3 0HA, UK

[17]European Southern Observatory, Alonso de C ordova 3107, Vitacura, Casilla 19001, Santiago 19, Chile

[18]Isaac Newton Group, Apartado de Correos 321, 38780 Santa Cruz de La Palma, Islas Canarias, Spain

[19]Department of Astronomy, University of Barcelona, Barcelona, Spain

[20]University of Texas, Department of Astronomy, C-1400, Austin, TX,78712, U.S.A.

1. Introduction

Five years ago, the Supernova Cosmology Project (SCP) and the High-Z Supernova Search both reported observations of Type Ia supernovae (SNe Ia), which gave strong evidence for an acceleration of the Universe's expansion, and hence for a non-zero cosmological constant, or dark energy density (Perlmutter *et al.* 1998; Garnavich *et al.* 1998a; Schmidt *et al.* 1998; Riess *et al.* 1998; Perlmutter *et al.* 1999, for a review, see Perlmutter & Schmidt 2003). These results ruled out a flat, matter-dominated ($\Omega_{\rm M} = 1$, $\Omega_\Lambda = 0$) universe. For a flat universe, motivated by inflation theory, these studies yielded a value for the cosmological constant of $\Omega_\Lambda \simeq 0.7$. Even in the absence of assumptions about the geometry of the Universe, the supernova results indicate at greater than a 99% confidence level the existence of dark energy.

The supernova results combined with observations of the power spectrum of the Cosmic Microwave Background (CMB) (e.g., Jaffe *et al.* 2001), the properties of massive clusters (e.g., Turner 2001; Allen, Schmidt, & Fabian 2002; Bahcall *et al.* 2003), and dynamical redshift-space distortions (Hawkins *et al.* 2002) yield a consistent picture of a flat universe with $\Omega_{\rm M} \simeq 0.3$ and $\Omega_\Lambda \simeq 0.7$ (Bahcall *et al.* 1999). Each of these measurements is sensitive to different combinations of the parameters, and hence they complement each other. Moreover, because there are three different measurements of two parameters, the combination provides an important consistency check. While the current observations of galaxy clusters and dynamics and high-redshift supernovae primarily probe the "recent" Universe at redshifts of $z < 1$, the CMB measurements probe the early Universe at $z \sim 1100$. That consistent results are obtained by measurements of vastly different epochs of the Universe's history is a vindication of the standard model of the expanding Universe.

In the redshift range around $z = 0.4$–0.7, the supernova results are most sensitive to a linear

[21]Department of Physics, University of Durham, South Road, Durham, DH1 3LE, UK

[22]National Astronomical Observatory, Mitaka, Tokyo 181-8588, Japan

[23]Now at LLR, CNRS-IN2P3, Ecole Polytechnique, Palaiseau, France

combination of Ω_M and Ω_Λ close to $\Omega_M \quad \Omega_\Lambda$. In contrast, galaxy clustering and dynamics are sensitive primarily to Ω_M alone, while the CMB is most sensitive to $\Omega_M + \Omega_\Lambda$. Although combinations of other measurements lead to a separate confirmation of the Universe's acceleration (e.g., Efstathiou *et al.* 2002), taken alone it is the supernovae that provide best the *direct* evidence for dark energy. Therefore, it is of importance to improve the precision of the supernova result, to confirm the result with additional independent high-redshift supernovae, and also to limit the possible effects of systematic errors.

Perlmutter *et al.* (1997, 1999) and Riess *et al.* (1998) presented extensive accounts of, and bounds for, possible systematic uncertainties in the supernova measurements. One obvious possible source of systematic uncertainty has been was discussed is the effect of host-galaxy dust. For a given mass density, the effect of a cosmological constant on the magnitudes of high-redshift supernovae is to make their observed brightness *dimmer* than would have been the case with $\Omega_\Lambda = 0$. Dust extinction from within the host galaxy of the high-redshift supernovae could have a similar effect; however, normal dust will also redden the colors of the supernovae. Therefore, a measurement of the color of the high-redshift supernovae, compared to the known colors of SNe Ia, has been used to provide an upper limit on the effect of host-galaxy dust extinction, or a direct measurement of that extinction which may then be corrected. Uncertainties on extinction corrections based on these color measurements usually dominate the statistical error of photometric measurements. Previous analyses have either selected a low-extinction subset of both low- and high-redshift supernovae and not applied corrections directly ("Fit C," the primary analysis of P99), or have used a biasing Bayesian prior on the intrinsic extinction distribution to limit the propagated uncertainties from errors in color measurements ("Fit E" of P99, Riess *et al.* 1998).

In Sullivan *et al.* (2003), we set stronger limits on the effects of host-galaxy extinction by comparing the extinction, cosmological parameters, and supernova peak magnitude dispersion for subsets of the SCP supernovae observed in different types of host galaxies, as identified from both HST imaging and Keck spectroscopy of the hosts. We found that supernovae in early-type (E and S0) galaxies show a smaller dispersion in peak magnitude at high redshift, as had previously been seen at low redshift (e.g. Wang, Hoeflich, & Wheeler 1997). This subset of the P99 sample— in hosts unlikely to be strongly affected by extinction— independently provided evidence at the 5σ level that $\Omega_\Lambda > 0$ in a flat Universe, confirming that host-galaxy dust extinction was unlikely to be a significant systematic in the results of P99. Although Sullivan *et al.* (2003) do present marginal evidence that high-redshift supernovae in late-type systems are systematically dimmer than those in early-type galaxies, even that offset is smaller than suggested in previous studies (e.g., Rowan-Robinson 2002) that suggests dust extinction as a primary contaminant leading to the interpretation of acceleration. Moreover, because it is only the difference between magnitudes of low-redshift and high-redshift supernovae that lead to the measurement of Ω_M and Ω_Λ, this offset does not affect those measurements; only were it found to systematically differ at different redshifts would introduce a systematic into Ω_M and Ω_Λ. The natural next step— presented in the current paper— is to provide high-quality individual unbiased $E(B\text{-}V)$ measurements which will allow us to directly measure the effect of host-galaxy extinction on each supernova event.

[For Saul and Greg to do: Find a wording of this that is more positive sounding from the beginning.]

[This sentence doesn't quite make it clear what distinguishes this next step from the previous Fit E and Riess et al work (but without going into repetitive detail that will be discussed later).

This paper presents eleven new supernovae discovered and observed by the SCP at redshifts $0.36 < z < 0.86$, a range very similar to that of the 42 high-redshift supernovae reported in Perlmutter *et al.* (1999, hereafter P99). The supernovae of that paper, with one exception, were observed entirely with ground-based telescopes; 11 of the 14 new supernovae reported by Riess *et al.* (1998) were also observed from the ground. The eleven supernovae of this work have lightcurves in both the R and I bands measured with the Wide-Field/Planetary Camera (WFPC2) on the Hubble Space Telescope (HST), and represent the largest sample to date of HST-measured SNe Ia at high redshift.

The HST provides two primary advantages for photometry of point sources such as supernovae. First the sky background is much lower, allowing a much higher signal-to-noise ratio in a single exposure. Second, because the telescope is not limited by atmospheric seeing, it has very high spa-

tial resolution. This helps the signal-to-noise ratio by greatly reducing the area of background emission which contributes to the noise of the source measurement, and moreover simplifies the task of separating the variable supernova signal from the host galaxy. With these advantages, the precision of the lightcurve and color measurements is much greater for the eleven supernovae in this paper than was possible for previous ground-based observations. These eleven supernovae themselves provide a high-precision *new* set of supernovae to test the accelerating universe results. Moreover, the higher precision lightcurve measurements in both R- and I-bands allow us to make high-quality, unbiased, individual host-galaxy extinction corrections to each supernova event.

We first describe the PSF-fit photometry method used for extracting the lightcurves from the WFPC2 images (§ 2.1). Next, in § 2.2, we describe the lightcurve fitting procedure, including the methods used for calculating accurate K-corrections. So that all supernovae may be treated consistently, in § 2.3 we apply the slightly updated K-correction procedure to all of the supernovae used in P99. In § 2.4, the cosmological fit methodology we use is described. In § 3, we discuss the evidence for host-galaxy extinction (only significant for one of the eleven new supernovae) from the R-I lightcurve colors. In § 4.1, we present the measurements of the cosmological parameters $\Omega_{\rm M}$ and Ω_Λ from the new dataset alone as well as combining this it with the data of P99. In § 4.2, we perform a combined fit with our data and the high-redshift SNe of Riess *et al.* (1998). Finally, we present measurements of w, the equation of state parameter for dark energy, from these data, and from these data combined with recent CMB and galaxy redshift distortion measurements in § 4.3. These discussions of our primary results are followed by updated analyses of systematic uncertainties are presented for these measurements in § 5.

2. Observations, Data Reduction, and Analysis

2.1. WFPC2 Photometry

The supernovae discussed in this paper are listed in Table 1. They were discovered during three different supernova searches, following the techniques described in Perlmutter *et al.* (1995, 1997, 1999). Two of the searches were conducted at the 4m Blanco telescope at the Cerro Tololo Inter-American Observatory (CTIO), in November/December 1997 and March/April 1998. The final search was conducted at the Canada-France-Hawaii Telescope (CFHT) on Mauna Kea in Hawaii in April/May 2000. In each case, 2–3 nights of reference images were followed 3–4 weeks later by 2–3 nights of search images. The two images of each search field were seeing-matched and subtracted, and were searched for residuals indicating a supernova candidate. Weather conditions limited the depth and hence the redshift range of the March/April 1998 search. Out of the three searches, eleven of the resulting supernova discoveries were followed with extensive HST photometry. These supernovae are spaced approximately evenly in the redshift range $0.3 < z < 0.9$. Nine out of the eleven supernovae were discovered very close to maximum light; two were discovered several days before maximum light.

Spectra were obtained with the red side of LRIS on the Keck 10m telescope (Oke *et al.* 1995), with FORS1 on Antu (VLT-UT1) (Appenzeller *et al.* 1998), and with EFOSC2[24] on the ESO 3.6m telescope. These spectra were used to confirm the identification of the candidates as SNe Ia, and to measure the redshift of each candidate. Nine of the eleven supernovae in the set have strong confirmation as Type Ia through the presence of Si II λ6150, Si II λ4190, or Fe II features that match those of a Type Ia observed at a similar epoch. SNe 1998ay and 1998be have spectra which are consistent with SNe Ia spectra, although this identification is less secure for those two. However, we note that the colors (measured at multiple epochs with the HST lightcurves) are inconsistent with other types. (We explore the systematic effect of removing those two supernovae from the set in § 5.2.)

Where possible, the redshift, z, of each candidate was measured by matching narrow features in the host galaxy of the supernovae; the precision of these measurements in z is typically 0.001. In cases where there were not sufficient host-galaxy features (SNe 1998aw and 1998ba), redshifts were measured from the supernova itself; in these cases, z is measured with a (conservative) precision of

[24] http://www.ls.eso.org/lasilla/sciops/efosc/

0.01 (Branch & van den Bergh 1993). Even in the latter case, redshift measurements do not contribute significantly to the uncertainties in the final cosmological measurements since these are dominated by the photometric uncertainties.

Each of these supernovae was imaged with two broadband filters using the Planetary Camera (PC) CCD of the WFPC2 on the HST, which has a scale of $0.046''$/pixel. Table 1 lists the dates of these observations. The F675W and F814W broadband filters were chosen to have maximum sensitivity to these faint objects, while being as close a match as practical to the rest-frame B and V filters at the targeted redshifts. (Note that all of our WFPC2 observing parameters except the exact target coordinates were fixed prior to the SN discoveries.) The effective system transmission curves provided by STScI indicate that, when used with WFPC2, F675W is most similar to ground-based R band while F814W is most similar to ground-based I band. These filters roughly correspond to redshifted B- and V-band filters for the supernovae at $z < 0.7$, and redshifted U- and B- band filters for the supernovae at $z > 0.7$.

The HST images were reduced through the standard HST "On-The-Fly Reprocessing" data reduction pipeline provided by the Space Telescope Science Institute. Images were then background subtracted, and images taken in the same orbit were combined to reject cosmic rays using the "crrej" procedure (a part of the STSDAS IRAF package). Photometric fluxes were extracted from the final images using a PSF-fitting procedure. Traditional PSF fitting procedures assume a single isolated point source above a constant background. In this case, the point source was superimposed on the image of the host galaxy. In all cases, the supernova image was separated from the core of the host galaxy; however, in most cases the separation was not enough that an annular measurement of the background would be accurate. Because the host-galaxy flux is the same in all of the images, we used a PSF fitting procedure that fits a PSF *simultaneously* to every image of a given supernova observed through a given photometric filter. The model we fit was:

$$f_i(x,y) = f_{0i} \times \mathrm{psf}(x \quad x_{0i}, y \quad y_{0i}) + \mathrm{bg}(x \quad x_{0i}, y \quad y_{0i}; a_j) + p_i \qquad (1)$$

where $f_i(x,y)$ is the measured flux in pixel (x,y) of the ith image, (x_{0i}, y_{0i}) is the position of the supernova on the ith image, f_{0i} is the total flux in the supernova in the ith image, $\mathrm{psf}(u,v)$ is a normalized point spread function, $\mathrm{bg}(u,v;a)$ is a temporally constant background parametrized by a_j, and p_i is a pedestal offset for the ith image. There are $4n + m \quad 1$ parameters in this model, where n is the number of images (typically 2, 5, or 6 previously summed images) and m is the number of parameters a_j that specify the background model (typically 3 or 6). (The $\quad 1$ is due to the fact that a zeroth-order term in the background is degenerate with one of the p_i terms.) Parameters varied include f_i, x_{0i}, y_{0i}, p_i, and a_j.

Due to the scarcity of objects in our PC images, geometric transformations between the images at different epochs using other objects on the four chips of WFPC2 together allowed an *a priori* determination of (x_{0i}, y_{0i}) good to ~ 1 pixel. Allowing those parameters to vary in the fit (effectively, using the point source signature of the supernova to determine the offset of the image) provided position measurements a factor of ~ 10 better.[25] The model was fit to 13×13 pixel patches extracted from all of the images of a time sequence of a single supernova in a single filter (except for SN 1998ay, which is close enough to the host galaxy that a 7×7 pixel patch was used to avoid having to fit the core of the galaxy with the background model). In four out of the 99 patches used in the fits to the 22 lightcurves, a single bad pixel was masked from the fit. The series of f_{0i} values, corrected as described in the rest of this section, provided the data used in the lightcurve fits described in § 2.2. For one supernova (SN 1997ek at $z = 0.86$), the F814W background was further constrained by a supernova-free "final reference" image taken 11 months after the supernova explosion.[26]

[25] Note that this may introduce a bias towards higher flux, as the fit will seek out positive fluctuations on which to center the PSF. However, the covariance between the peak flux and position is typically less than $\sim 4\%$ the position uncertainty times the flux uncertainty, so the effects of this bias will be very small in comparison to our photometric errors.

[26] Although obtaining final references to subtract the galaxy background is standard procedure for ground-based photometry of high-redshift supernovae, the higher resolution of WFPC2 provides sufficient separation between the supernova and host galaxy that such images are not always

Table 1: WFPC2 Supernova Observations

SN Name	z	F675W Observations	F814W Observations
1997ek	0.863	1998-01-05 (400s,400s)	1998-01-05 (500s,700s)
		1998-01-11 (400s,400s)	1998-01-11 (500s,700s)
			1998-02-02 (1100s,1200s)
			1998-02-14 (1100s,1200s)
			1998-02-27 (1100s,1200s)
			1998-11-09 (1100s,1300s)
			1998-11-16 (1100s,1300s)
1997eq	0.538	1998-01-06 (300s,300s)	1998-01-06 (300s,300s)
		1998-01-21 (400s,400s)	1998-01-11 (300s,300s)
			1998-02-02 (500s,700s)
		1998-02-11 (400s,400s)	1998-02-11 (500s,700s)
		1998-02-19 (400s,400s)	1998-02-19 (500s,700s)
1997ez	0.778	1998-01-05 (400s,400s)	1998-01-05 (500s,700s)
		1998-01-11 (400s,400s)	1998-01-11 (500s,700s)
			1998-02-02 (1100s,1200s)
			1998-02-14 (1100s,1200s)
			1998-02-27 (100s,1200s,1100s,1200s)
1998as	0.355	1998-04-08 (400s,400s)	1998-04-08 (500s,700s)
		1998-04-20 (400s,400s)	1998-04-20 (500s,700s)
		1998-05-11 (400s,400s)	1998-05-11 (500s,700s)
		1998-05-15 (400s,400s)	1998-05-15 (500s,700s)
		1998-05-29 (400s,400s)	1998-05-29 (500s,700s)
1998aw	0.440	1998-04-08 (300s,300s)	1998-04-08 (300s,300s)
		1998-04-18 (300s,300s)	1998-04-18 (300s,300s)
		1998-04-29 (400s,400s)	1998-04-29 (500s,700s)
		1998-05-14 (400s,400s)	1998-05-14 (500s,700s)
		1998-05-28 (400s,400s)	1998-05-28 (500s,700s)
1998ax	0.497	1998-04-08 (300s,300s)	1998-04-08 (300s,300s)
		1998-04-18 (300s,300s)	1998-04-18 (300s,300s)
		1998-04-29 (300s,300s)	1998-04-29 (500s,700s)
		1998-05-14 (300s,300s)	1998-05-14 (500s,700s)
		1998-05-27 (300s,300s)	1998-05-27 (500s,700s)
1998ay	0.638	1998-04-08 (400s,400s)	1998-04-08 (500s,700s)
		1998-04-20 (400s,400s)	1998-04-20 (500s,700s)
			1998-05-11 (1100s,1200s)
			1998-05-15 (1100s,1200s)
			1998-06-03 (1100s,1200s)
1998ba	0.430	1998-04-08 (300s,300s)	1998-04-08 (300s,300s)
		1998-04-19 (300s,300s)	1998-04-19 (300s,300s)
		1998-04-29 (400s,400s)	1998-04-29 (500s,700s)
		1998-05-13 (400s,400s)	1998-05-13 (500s,700s)
		1998-05-28 (400s,400s)	1998-05-28 (500s,700s)
1998be	0.644	1998-04-08 (300s,300s)	1998-04-08 (300s,300s)
		1998-04-19 (300s,300s)	1998-04-19 (300s,300s)
		1998-04-30 (400s,400s)	1998-04-30 (500s,700s)
		1998-05-15 (400s,400s)	1998-05-15 (500s,700s)
		1998-05-28 (400s,400s)	1998-05-28 (500s,700s)
1998bi	0.740	1998-04-06 (400s,400s)	1998-04-06 (500s,700s)
		1998-04-18 (400s,400s)	1998-04-18 (500s,700s)
			1998-04-28 (1100s,1200s)
			1998-05-12 (1100s,1200s)
			1998-06-02 (1100s,1200s)
2000fr	0.543		2000-05-08 (2200s)
		2000-05-15 (600s,600s)	2000-05-15 (1100s,1100s)
		2000-05-28 (600s,600s)	2000-05-28 (600s,600s)
		2000-06-10 (500s,500s)	2000-06-10 (600s,600s)
		2000-06-22 (1100s,1300s)	2000-06-22 (1100s,1200s)
		2000-07-08 (1100s,1300s)	2000-07-08 (110s,1200s)

A single Tiny Tim PSF was used as $\mathrm{psf}(u, v)$ for all images of a given band. The Tiny Tim PSF used was subsampled to 10×10 subpixels; in the fit procedure, it was shifted and integrated (properly summing fractional subpixels). After shifting and resampling to the PC pixel scale, it was convolved with an empirical 3×3 electron diffusion kernel with 75% of the flux in the central element Fruchter (2000).[27] To ensure proper photometry, the PSF was normalized in a $0.5''$-radius aperture, chosen to match the standard zeropoint calibration (Holtzman, *et al.* 1995; Dolphin 2000). Although the use of a single PSF for every image is an approximation— the PSF of WFPC2 depends on the epoch of the observation as well as the position on the CCD— this approximation should be valid, especially given that for all of the observations the supernova was positioned close to the center of the PC. To verify that this approximation is valid, we reran the PSF fitting procedure with individually generated PSFs for most supernovae; we also explored using a supernova spectrum instead of a standard star spectrum in generating the PSF. The measured fluxes were not significantly different, showing differences in both directions generally within 1–2% of the supernova peak flux value — much less than our photometric uncertainties on individual data points.

Although one of the great advantages of the Hubble Space Telescope is its low background, CCD photometry of faint objects over a low background suffer from an imperfect charge transfer efficiency (CTE) effect, which can lead to a systematic underestimate of the flux of point sources (Whitemore, Heyer, & Casertano 1999; Dolphin 2000, 2003). On the PC, these effects can be as large as $\sim 15\%$. The measured flux values (f_i above) were corrected for the CTE of WFPC2 following the standard procedure of Dolphin (2000).[28] Because the host galaxy is a smooth background underneath the point source, it was considered as a contribution to the background in the CTE correction. For an image which was a combination of several separate exposures within the same orbit or orbits, the CTE calculation was performed assuming that each SN image had a measured SN flux whose fraction of the total flux was equal to the fraction of that individual image's exposure time to the summed image's total exposure time. This assumption is correct most of the time, with the exception of the few instances where Earthshine affects part of an orbit.

In addition to the HST data, there exists ground-based photometry for each of these supernovae. This includes the images from the search itself, as well as a limited amount of follow-up. The details of which supernovae were observed with which telescopes are given with the lightcurves in Appendix A. Ground-based photometric fluxes were extracted from images using the same aperture photometry procedure of P99. A complete lightcurve in a given filter (R or I) combined the HST data with the ground-based data (using the color correction procedure described below in § 2.3), using measured zeropoints for the ground-based data and the Vega zeropoints of Dolphin (2000) for the HST data. The uncertainties on those zeropoints (0.003 for F814W or 0.006 for F675W) were added as correlated errors between all HST data points when combining with the ground-based lightcurve. Similarly, the measured uncertainty in the ground-based zeropoint was added as a correlated error to all ground-based fluxes. Ground based photometric calibrations were based on observations of Landolt (1992) standard stars observed on the same photometric night as a supernova observation; each calibration is confirmed over two or more nights. Ground-based zeropoint uncertainties are generally $\lesssim 0.02$–0.3; the R-band ground based zeropoint for SN 1998ay is only good to ± 0.05.

2.2. Lightcurve Fits

It is the magnitude of the supernova at its lightcurve peak that serves as a "calibrated candle" in estimating the cosmological parameters from the luminosity distance relationship. To estimate this peak magnitude, we performed template fits to the time series of photometric data for each supernova. In addition to the eleven supernovae described here, lightcurve fits were also performed to the supernovae from P99, including 18 supernovae from Hamuy *et al.* (1996a, hereafter H96), and eight from Riess *et al.* (1999a, hereafter R99)

necessary, particularly in this redshift range.

[27] See also http://www.stsci.edu/software/tinytim/tinytim_faq.html

[28] These CTE corrections used updated coefficients posted on Dolphin's web page (http://www.noao.edu/staff/dolphin/wfpc2_calib/) in September, 2002.

which match the same selection criteria used for the H96 supernovae (having data within six days of maximum light and located at $cz > 4000$ km/s, limiting distance modulus error due to peculiar velocities to less than 0.15 magnitudes). Because of new templates and K-corrections (see below), lightcurve fits to the photometric data on the 35 of the 42 high-redshift supernovae of P99 were redone for consistency. (Seven supernovae from P99 do not have a color measurement, and for that reason are not included in any of the analyses in this paper. These include SNe 1992bi, 1994F, 1994H, 1994al, 1994am, 1994an, and 1997L.)

Lightcurve fits were performed using a χ^2-minimization procedure based on MINUIT (James & Roos 1975). For both high- and low-redshift supernovae, color corrections and K-corrections are applied (see § 2.3) to the photometric data. These data were then fit to lightcurve templates. Fits were performed to the combined R- and I-band data for each high-redshift supernova. For low-redshift supernovae, fits were performed using only the B- and V-band data (which correspond to deredshifted R- and I-bands for most of the high-redshift supernovae). The lightcurve model fit to the supernova has four parameters to modify the lightcurve templates: time of rest-frame B-band maximum light, peak flux in R, R-I color at the epoch of rest-frame maximum B-band light, and timescale stretch s. Stretch is a parameter which linearly scales the time axis, so that a supernova with a high stretch has a relatively slow decay from maximum, and a supernova with a low stretch has a relatively fast decay from maximum(Perlmutter *et al.* 1997; Goldhaber *et al.* 2001). For supernovae in the redshift range $z = 0.3$–0.7, a B template was fit to the R-band lightcurve and a V template was fit to the I-band lightcurve. For supernovae at $z > 0.7$, a U template was fit to the R-band lightcurve and a B template to the I-band lightcurve. Two of the high-redshift supernovae from P99 fall at $z \sim 0.18$ (SN 1997I and SN 1997N); for these supernovae, V and R templates were fit to the R and I band data. (The peak B band magnitude was extracted by adding the intrinsic SN Ia B-V color to the fit V band magnitude at the epoch of B maximum.)

The B template used in the lightcurve fits was that of Goldhaber *et al.* (2001). For this paper, new V-band and R-band templates were generated following a procedure similar to that of Goldhaber *et al.* (2001), by fitting a smooth parametrized curve through the low-redshift supernova data of H96 and R99. A new U-band template was generated with data from Hamuy *et al.* (1991), Lira *et al.* (1998), Richmond *et al.* (1995), Suntzeff *et al.* (1999), and Wells *et al.* (1994); comparison of our U-band template shows good agreement with the new U-band photometry from Jha (2002) at the relevant epochs. New templates were generated by fitting a smooth curve, $f(t')$, to the the low-redshift lightcurve data, where $t' = t/(1+z)/s$; t is the number of days relative to the epoch of the B-band maximum of each supernova, z is the redshift of each supernova, and s is the stretch of each supernova as measured from the B-band lightcurves. Lightcurve templates had an initial parabola with a 20-day rise time (Aldering, Knop, & Nugent 2000), joined to a smooth spline section to describe the main part of the lightcurve, then joined to an exponential decay to describe the final tail at $>\sim 70$ days past maximum light. The first 100 days of each of the three templates is listed in Table 2.

Due to a secondary "hump" or "shoulder" ~ 20 days after maximum, the R-band lightcurve does not vary strictly according to the single simple stretch parameter which is so successful in describing the different U-, B-, and V-band lightcurves. However, for the two $z \sim 0.18$ supernova to which we fit an R-band template, the peak R- and I-band magnitudes are well constrained, and the stretch is also well measured from the R-band (rest frame V-band) lightcurve.

Some of the high-redshift supernovae from P99 lack a supernova-free host-galaxy image. These supernovae were fit with an additional variable parameter: the zero-level of the I-band lightcurve. The supernovae treated in this manner include SNe 1997J, 1997O, 1997Q, 1997R, SN 1997S, SN 1997K, and 1997am. Both R- and I-band zero offsets were allowed to vary for SN 1994G.

The late-time lightcurve behavior may bias the result of a lightcurve fit (Aldering, Knop, & Nugent 2000); it is therefore important that the low- and high-redshift supernovae be treated in as consistent a manner as possible. Few or none of the high-redshift supernovae have high-precision measurements more than $\sim$40–50 rest-frame days

Table 2: U, V, and R Lightcurve Templates Used

Day[a]	U flux[b]	V flux[b]	R flux[b]	Day[1]	U flux[b]	V flux[b]	R flux[b]
-19	6.712e-03	4.960e-03	5.779e-03	31	4.790e-02	2.627e-01	3.437e-01
-18	2.685e-02	1.984e-02	2.312e-02	32	4.524e-02	2.481e-01	3.238e-01
-17	6.041e-02	4.464e-02	5.201e-02	33	4.300e-02	2.345e-01	3.054e-01
-16	1.074e-01	7.935e-02	9.246e-02	34	4.112e-02	2.218e-01	2.887e-01
-15	1.678e-01	1.240e-01	1.445e-01	35	3.956e-02	2.099e-01	2.733e-01
-14	2.416e-01	1.785e-01	2.080e-01	36	3.827e-02	1.990e-01	2.592e-01
-13	3.289e-01	2.430e-01	2.832e-01	37	3.722e-02	1.891e-01	2.463e-01
-12	4.296e-01	3.174e-01	3.698e-01	38	3.636e-02	1.802e-01	2.345e-01
-11	5.437e-01	4.017e-01	4.681e-01	39	3.565e-02	1.721e-01	2.237e-01
-10	6.712e-01	4.960e-01	5.779e-01	40	3.506e-02	1.649e-01	2.137e-01
-9	7.486e-01	5.889e-01	6.500e-01	41	3.456e-02	1.583e-01	2.046e-01
-8	8.151e-01	6.726e-01	7.148e-01	42	3.410e-02	1.524e-01	1.962e-01
-7	8.711e-01	7.469e-01	7.725e-01	43	3.365e-02	1.471e-01	1.884e-01
-6	9.168e-01	8.115e-01	8.236e-01	44	3.318e-02	1.423e-01	1.813e-01
-5	9.524e-01	8.660e-01	8.681e-01	45	3.266e-02	1.378e-01	1.747e-01
-4	9.781e-01	9.103e-01	9.062e-01	46	3.205e-02	1.337e-01	1.687e-01
-3	9.940e-01	9.449e-01	9.382e-01	47	3.139e-02	1.299e-01	1.630e-01
-2	1.000e+00	9.706e-01	9.639e-01	48	3.072e-02	1.263e-01	1.578e-01
-1	9.960e-01	9.880e-01	9.834e-01	49	3.005e-02	1.229e-01	1.529e-01
0	9.817e-01	9.976e-01	9.957e-01	50	2.945e-02	1.195e-01	1.483e-01
1	9.569e-01	1.000e+00	1.000e+00	51	2.893e-02	1.161e-01	1.440e-01
2	9.213e-01	9.958e-01	9.952e-01	52	2.853e-02	1.128e-01	1.398e-01
3	8.742e-01	9.856e-01	9.803e-01	53	2.830e-02	1.096e-01	1.359e-01
4	8.172e-01	9.702e-01	9.545e-01	54	2.827e-02	1.064e-01	1.320e-01
5	7.575e-01	9.502e-01	9.196e-01	55	2.849e-02	1.033e-01	1.282e-01
6	6.974e-01	9.263e-01	8.778e-01	56	2.793e-02	1.003e-01	1.244e-01
7	6.375e-01	8.991e-01	8.313e-01	57	2.738e-02	9.743e-02	1.207e-01
8	5.783e-01	8.691e-01	7.821e-01	58	2.684e-02	9.467e-02	1.170e-01
9	5.205e-01	8.369e-01	7.324e-01	59	2.630e-02	9.207e-02	1.133e-01
10	4.646e-01	8.031e-01	6.842e-01	60	2.578e-02	8.964e-02	1.097e-01
11	4.113e-01	7.683e-01	6.396e-01	61	2.527e-02	8.741e-02	1.061e-01
12	3.610e-01	7.330e-01	6.007e-01	62	2.477e-02	8.538e-02	1.026e-01
13	3.145e-01	6.977e-01	5.691e-01	63	2.428e-02	8.359e-02	9.910e-02
14	2.725e-01	6.629e-01	5.444e-01	64	2.380e-02	8.207e-02	9.568e-02
15	2.356e-01	6.293e-01	5.254e-01	65	2.333e-02	8.083e-02	9.232e-02
16	2.044e-01	5.972e-01	5.113e-01	66	2.287e-02	7.927e-02	8.902e-02
17	1.783e-01	5.667e-01	5.011e-01	67	2.242e-02	7.774e-02	8.579e-02
18	1.567e-01	5.376e-01	4.938e-01	68	2.197e-02	7.624e-02	8.264e-02
19	1.388e-01	5.099e-01	4.887e-01	69	2.154e-02	7.476e-02	7.958e-02
20	1.239e-01	4.835e-01	4.848e-01	70	2.111e-02	7.332e-02	7.660e-02
21	1.115e-01	4.583e-01	4.814e-01	71	2.070e-02	7.191e-02	7.373e-02
22	1.008e-01	4.342e-01	4.776e-01	72	2.029e-02	7.052e-02	7.096e-02
23	9.144e-02	4.113e-01	4.725e-01	73	1.989e-02	6.916e-02	6.832e-02
24	8.314e-02	3.894e-01	4.653e-01	74	1.949e-02	6.782e-02	6.581e-02
25	7.583e-02	3.685e-01	4.552e-01	75	1.911e-02	6.651e-02	6.344e-02
26	6.941e-02	3.486e-01	4.414e-01	76	1.873e-02	6.523e-02	6.199e-02
27	6.380e-02	3.296e-01	4.247e-01	77	1.836e-02	6.397e-02	6.057e-02
28	5.891e-02	3.115e-01	4.058e-01	78	1.799e-02	6.274e-02	5.918e-02
29	5.467e-02	2.943e-01	3.855e-01	79	1.764e-02	6.153e-02	5.783e-02
30	5.102e-02	2.781e-01	3.645e-01	80	1.729e-02	6.034e-02	5.650e-02

a: Day is relative to the epoch of the maximum of the B-band lightcurve. The B-band template may be found in Goldhaber *et al.* (2001).
b: Relative fluxes.

after maximum light, so as in Perlmutter *et al.* (1997) and P99 these late-time points were eliminated from the low-redshift lightcurve data before the template-fit procedure. Additionally, to allow for systematic offset uncertainties on the host-galaxy subtraction, an "error floor" of 0.007 times the maximum lightcurve flux was applied; any lightcurve point with an uncertainty below the error floor had its uncertainty replaced by that value (Goldhaber *et al.* 2001).

The final results of the lightcurve fits, including the effect of color corrections and K-corrections, are listed in Table 3 for the eleven supernovae of this paper. Table 4 shows the results of new lightcurve fits for 35 of the high-redshift supernovae of P99, and Table 5 shows the results of lightcurve fits for the low-redshift supernovae from H96 and R99. Appendix A tabulates all of the lightcurve data for the eleven HST supernovae in this paper. The lightcurves for these supernovae (and the F675W WFPC2 image nearest maximum light) are shown in Figures 1 and 2. Note that there are correlated errors between all of the ground-based points in these figures, as a single ground-based zeropoint was used to scale them together with the HST photometry.

For some of the highest-redshift supernovae, there are small systematic offsets between the K-corrected ground-based and HST photometry in the R-band. Because the HST photometry has much greater statistical weight in the fit, this systematic offset manifests itself as ground-based points systematically above the lightcurve fit. The most likely source of these offsets are the color corrections between the ground-based R-band and F675W filters, which have different transmission functions. These corrections are calculated from integrations of spectrophotometry of well-studied low-redshift SNe Ia (see § 2.3). For the higher redshifts, those integrations include the U-band region of the spectrum, where there is not currently as much high-quality spectrophotometry available as at longer wavelengths. These offsets will not greatly affect any of our primary cosmological fits, since at the higher redshifts the rest-frame peak B-band magnitude is estimated from the observed I-band lightcurve (where there is no evidence for a systematic difference between ground- and space-based data). The effect that a different U-band spectral template would have both on our K-corrections and on our color excesses will be considered in § 5.4.

2.3. Color- and K-Corrections

In order to combine data from different telescopes, color corrections were applied to remove the differences in the spectral responses of the filters relative to the Bessell system (Bessell 1990). For the ground-based telescopes, the filters are close enough to the standard Bessell filters that a single linear color term (measured at each observatory with standard stars) suffices to put the data onto the Bessell system, with most corrections being smaller than 0.01 magnitudes. The WFPC2 filters are different enough from the ground-based filters, however, that a linear term is not sufficient. Moreover, the differences between a SN Ia and standard star spectral energy distribution (SED) are significant. In this case, color corrections were calculated by integrating template SN Ia spectra (described below).

In order to perform lightcurve template fitting, a cross-filter K-correction must be applied to transform the data in the observed filter into a rest-frame magnitude in the filter used for the lightcurve template (Kim, Goobar, & Perlmutter 1996). The color correction to the nearest standard Bessell filter followed by a K-correction to a rest-frame filter is equivalent to a direct K-correction from the observed filter to the standard rest-frame filter. In practice, we perform the two steps separately so that all photometry may be combined to provide a lightcurve effectively observed through a standard (e.g.) R-band filter, which may then be K-corrected and fit with a single series of K-corrections. The data tabulated in Appendix A have all been color-corrected to the standard Bessell filters.

Color and K-corrections were performed following the procedure of Nugent, Kim, & Perlmutter (2002). In order to perform these corrections, a template SN Ia spectrum for each epoch of the lightcurve, as described in that paper, is necessary. The spectral template used in this present work began with the template of that paper. To it was applied a smooth multiplicative function at each day such that integration of the spectrum through the standard filters would produce the proper intrinsic colors for a Type Ia supernova (including a mild dependence of those intrinsic colors

IMPORTANT suggestion: Make the HST points the filled black circles and the ground-based points the open empty circles, since the black points are the more important ones to emphasize. Also, I think these plot would look better if we make all the points smaller than they are currently.

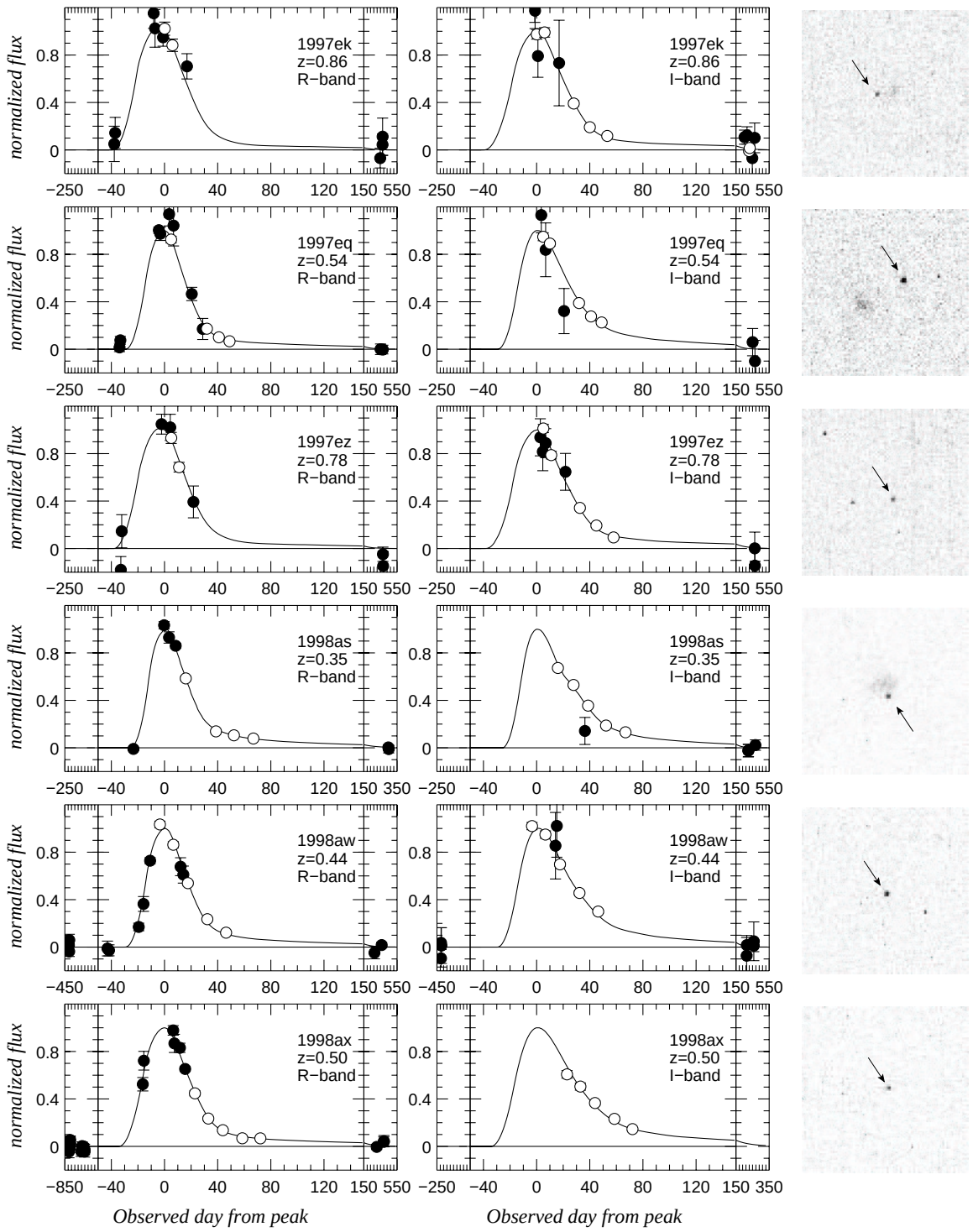

Fig. 1.— Lightcurves and images from the PC CCD on WFPC2 for the HST supernovae reported in this paper. The left column shows the R-band (including F675W HST data), the middle column I-band lightcurves (including F814W HST data), and the right column $7'' \times 7''$ F675W images of the supernovae. Filled circles represent ground-based data points, and open circles represent WFPC2 data points.

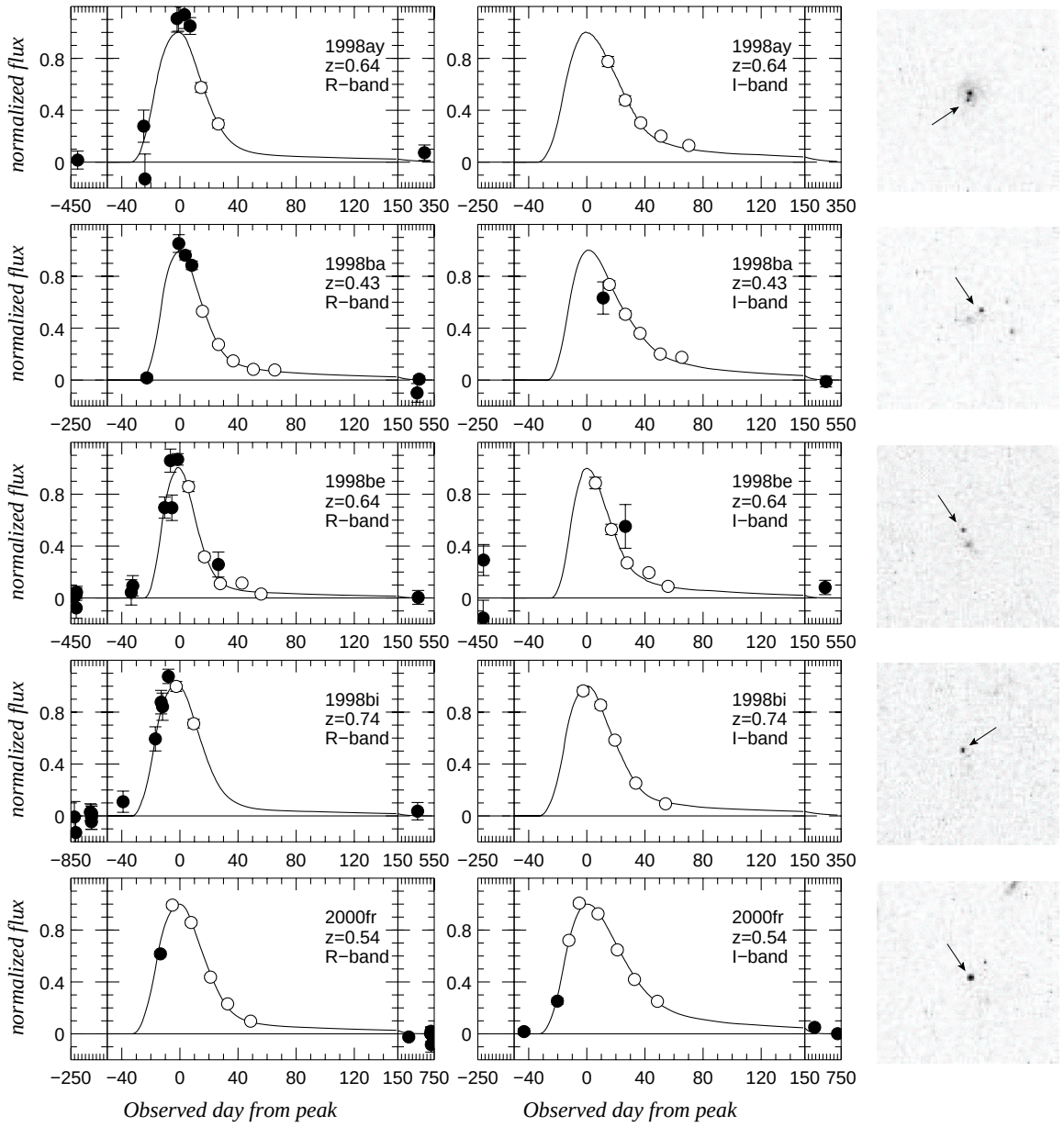

Fig. 2.— Lightcurves and images from the PC CCD on WFPC2 for the HST supernovae reported in this paper. The left column shows the R-band (including F675W HST data), the middle column I-band lightcurves (including F814W HST data), and the right column $7'' \times 7''$ F675W images of the supernovae. Filled circles represent ground-based data points, and open circles represent WFPC2 data points.

Table 3: Supernova Lightcurve Fits: HST Supernovae from this paper

SN	z	m_X[a]	m_B[b]	Stretch	R-I[c]	$E(B\text{-}V)$ Gal.[d]	$E(B\text{-}V)^e_{\rm host}$	Excluded from Subsets[f]
1997ek	0.863	23.31	24.51 ± 0.03	1.063 ± 0.078	0.835 ± 0.059	0.042	0.094 ± 0.083	
1997eq	0.538	22.63	23.21 ± 0.02	0.958 ± 0.027	0.201 ± 0.030	0.044	0.034 ± 0.034	
1997ez	0.778	23.17	24.29 ± 0.04	1.079 ± 0.035	0.701 ± 0.049	0.026	0.094 ± 0.069	
1998as	0.355	22.18	22.73 ± 0.03	0.953 ± 0.019	0.237 ± 0.028	0.037	0.178 ± 0.031	2,3
1998aw	0.440	22.56	23.22 ± 0.02	1.026 ± 0.019	0.304 ± 0.024	0.026	0.264 ± 0.026	1–3
1998ax	0.497	22.63	23.25 ± 0.05	1.150 ± 0.032	0.210 ± 0.041	0.035	0.110 ± 0.044	2,3
1998ay	0.638	23.26	23.86 ± 0.08	1.038 ± 0.046	0.333 ± 0.069	0.035	0.006 ± 0.086	3
1998ba	0.430	22.35	22.97 ± 0.03	0.954 ± 0.021	0.098 ± 0.036	0.024	0.047 ± 0.038	
1998be	0.644	23.29	23.86 ± 0.04	0.753 ± 0.029	0.450 ± 0.051	0.029	0.123 ± 0.065	2,3
1998bi	0.740	22.85	23.92 ± 0.02	0.950 ± 0.030	0.552 ± 0.037	0.026	0.027 ± 0.050	
2000fr	0.543	22.44	23.06 ± 0.02	1.062 ± 0.012	0.134 ± 0.022	0.030	0.033 ± 0.025	

a: Magnitude in the observed filter at the peak of the rest-frame B-band lightcurve. X=R for $z < 0.7$, X=I for $z > 0.7$.
b: This value has been K-corrected and corrected for Galactic extinction.
c: This is the observed R-I color at the epoch of the rest-frame B-band lightcurve peak.
d: Schlegel, Finkbeiner, & Davis (1998)
e: Measurement uncertainty only; no intrinsic color dispersion included.
f: These supernovae are excluded from the indicated subsets; see § 2.5.

I think this was pretty clear (and less worrying) without this parenthetical explanation.

on stretch).

The proper intrinsic colors for the supernova spectral template were determined in the $BVRI$ spectral range by smooth fits to the low-redshift supernova data of H96 and R99. For each color (B-V, V-R, and R-I), every data point from those papers was K-corrected and corrected for Galactic extinction. These data were plotted together, and then a smooth curve was fit to the plot of color versus date relative to maximum. This curve is given by two parameters, each of which is a function of time and is described by a spline under tension: an "intercept" $b(t)$ and a "slope" $m(t)$. At any given date the intrinsic color is

$$color(t') = b(t') + m(t') \times (1/s \quad 1) \qquad (2)$$

where $t' = t/(s(1+z))$, z is the redshift of the supernova, and s is the timescale stretch of the supernova from a simultaneous fit to the B and V lightcurves (matching the procedure used for most of the high-redshift supernovae). As the goal was to determine intrinsic colors without making any assumptions about reddening, no host-galaxy extinction corrections were applied to the literature data at this stage of the analysis. Instead, host-galaxy extinction was handled by fitting the blue side ridge-line of the supernova color curves, so as to extract the unreddened intrinsic color. This ridge-line fit was performed by adding an asymmetric intrinsic error bar of 0.04 on the red side, and 0.12 to the blue side ~~(i.e., so that the fit would prefer to have the model be bluer rather than redder in comparison to the points, as supernovae may be reddened due to host galaxy extinction).~~ The blue-side error bar was also extendable, in that the χ^2 minimization treated a point redward of the fit by $> 1\sigma$ as only exactly 1σ away. Finally, those supernovae which were most reddened (with $E(B\text{-}V) > 0.2$) were omitted. The resulting fit procedure provided B-V, V-R, and R-I as a function of epoch and stretch; those colors were used to correct the template spectrum as described above.

[Why do you call this extendable? And why "blue-side" when it is the red side that is affected?]

Some of our data extend into the U-band range of the spectrum. This is obvious for supernovae at $z > 0.7$ where a U-band template is fit to the R-band data. However, even for supernovae at $z \gtrsim 0.55$, the de-redshifted R-band filter begins to overlap the U-band range of the rest-frame spectrum. Thus, it is also important to know the intrinsic U-B color so as to generate a proper spectral template. We used data from the literature in Table 6. Here, there is an insufficient number of supernova lightcurves to reasonably use the sort of ridge-line analysis used above to eliminate the effects of host-galaxy extinction in determining the intrinsic $BVRI$ colors. Instead, for U-B, we perform extinction corrections using the $E(B\text{-}V)$ values from Phillips *et al.* (1999). Based on Table 6, we adopt a U-B color of 0.4 at the epoch of rest-B maximum. This value is also consistent with the data shown in Jha (2002) for supernovae with timescale stretch of $s \sim 1$, although

Table 4: Supernova Lightcurve Fits: New Fits to Perlmutter (1999) SNe

SN	z	m_X [a]	m_B [b]	Stretch	R-I [c]	$E(B\text{-}V)$ Gal. [d]	$E(B\text{-}V)^e_{\rm host}$	Excluded from Subsets [f]
1994G	0.425	21.70	22.38 ± 0.07	0.873 ± 0.100	0.159 ± 0.151	0.008	0.115 ± 0.161	1–3
1995aq	0.453	22.61	23.25 ± 0.07	0.869 ± 0.100	0.035 ± 0.133	0.022	0.049 ± 0.140	1–3
1995ar	0.465	22.79	23.48 ± 0.08	0.906 ± 0.104	0.509 ± 0.242	0.022	0.451 ± 0.263	
1995as	0.498	23.03	23.69 ± 0.07	1.036 ± 0.091	0.155 ± 0.205	0.021	0.051 ± 0.221	3
1995at	0.655	22.63	23.25 ± 0.04	1.040 ± 0.064	0.383 ± 0.112	0.019	0.038 ± 0.141	1–3
1995aw	0.400	21.78	22.29 ± 0.03	1.196 ± 0.038	0.125 ± 0.104	0.040	0.152 ± 0.108	
1995ax	0.615	22.56	23.22 ± 0.06	1.112 ± 0.077	0.151 ± 0.213	0.033	0.156 ± 0.259	
1995ay	0.480	22.64	23.07 ± 0.04	0.880 ± 0.066	0.208 ± 0.164	0.114	0.049 ± 0.176	
1995az	0.450	22.46	22.70 ± 0.07	0.973 ± 0.066	0.087 ± 0.138	0.181	0.087 ± 0.147	
1995ba	0.388	22.07	22.64 ± 0.06	0.971 ± 0.047	0.015 ± 0.106	0.018	0.019 ± 0.112	
1996cf	0.570	22.71	23.31 ± 0.03	0.996 ± 0.048	0.162 ± 0.093	0.040	0.055 ± 0.108	3
1996cg	0.490	22.46	23.09 ± 0.03	1.011 ± 0.041	0.300 ± 0.101	0.035	0.204 ± 0.109	3
1996ci	0.495	22.19	22.83 ± 0.02	0.964 ± 0.043	0.083 ± 0.071	0.028	0.033 ± 0.076	
1996ck	0.656	23.11	23.77 ± 0.06	0.871 ± 0.090	0.214 ± 0.264	0.032	0.197 ± 0.332	
1996cl	0.828	23.37	24.53 ± 0.17	0.973 ± 0.242	0.549 ± 0.189	0.035	0.344 ± 0.257	
1996cm	0.450	22.67	23.27 ± 0.07	0.898 ± 0.065	0.216 ± 0.180	0.049	0.131 ± 0.192	3
1996cn	0.430	22.58	23.26 ± 0.03	0.892 ± 0.063	0.379 ± 0.091	0.025	0.339 ± 0.099	1–3
1997F	0.580	22.93	23.51 ± 0.06	1.040 ± 0.066	0.275 ± 0.205	0.040	0.062 ± 0.242	
1997G	0.763	23.46	24.43 ± 0.39	0.864 ± 0.110	0.124 ± 0.463	0.043	0.658 ± 0.609	
1997H	0.526	22.70	23.26 ± 0.03	0.883 ± 0.049	0.299 ± 0.181	0.051	0.148 ± 0.202	
1997I	0.172	20.18	20.37 ± 0.01	0.968 ± 0.009	0.063 ± 0.047	0.051	0.060 ± 0.064	
1997J	0.619	23.23	23.86 ± 0.06	1.023 ± 0.109	0.190 ± 0.341	0.039	0.127 ± 0.417	
1997K	0.592	23.79	24.42 ± 0.12	1.076 ± 0.158	0.301 ± 0.356	0.020	0.084 ± 0.425	1–3
1997N	0.180	20.39	20.41 ± 0.02	1.067 ± 0.016	0.136 ± 0.095	0.031	0.159 ± 0.125	
1997O	0.374	22.99	23.54 ± 0.07	1.047 ± 0.072	0.093 ± 0.157	0.029	0.060 ± 0.167	1–3
1997P	0.472	22.53	23.16 ± 0.04	0.888 ± 0.039	0.057 ± 0.218	0.033	0.048 ± 0.230	
1997Q	0.430	22.01	22.61 ± 0.02	0.935 ± 0.024	0.065 ± 0.144	0.030	0.006 ± 0.152	
1997R	0.657	23.29	23.89 ± 0.05	0.940 ± 0.059	0.392 ± 0.181	0.030	0.032 ± 0.229	
1997S	0.612	23.04	23.87 ± 0.05	1.158 ± 0.064	0.398 ± 0.421	0.033	0.808 ± 0.502	
1997ac	0.320	21.42	21.88 ± 0.02	1.063 ± 0.020	0.071 ± 0.066	0.027	0.020 ± 0.073	
1997af	0.579	22.94	23.60 ± 0.07	0.853 ± 0.050	0.047 ± 0.238	0.028	0.209 ± 0.279	
1997ai	0.450	22.34	22.93 ± 0.05	0.790 ± 0.086	0.144 ± 0.137	0.045	0.042 ± 0.145	
1997aj	0.581	22.58	23.24 ± 0.07	0.948 ± 0.047	0.047 ± 0.170	0.033	0.210 ± 0.200	
1997am	0.416	22.01	22.59 ± 0.07	1.032 ± 0.066	0.040 ± 0.114	0.036	0.002 ± 0.120	
1997ap	0.830	23.16	24.35 ± 0.06	1.023 ± 0.063	0.903 ± 0.083	0.026	0.155 ± 0.119	

a: X=R for $z < 0.7$, X=I for $z > 0.7$
b: As in Table 3
c: As in Table 3
d: Schlegel, Finkbeiner, & Davis (1998)
e: As in Table 3
f: These supernovae are excluded from the indicated subsets; see § 2.5.

Table 5: Supernova Lightcurve Fits: Low-z SNe from Hamuy (1996) and Riess (1999)

SN[a]	z	m_B[b]	m_B[c]	Stretch	B-V[d]	$E(B\text{-}V)$ Gal.[e]	$E(B\text{-}V)_{\rm host}$	Excluded from Subsets[f]
1990O	0.030	16.58	16.18 ± 0.03	1.106 ± 0.026	0.041 ± 0.026	0.098	0.001 ± 0.027	
1990af	0.050	17.92	17.76 ± 0.01	0.751 ± 0.010	0.077 ± 0.011	0.035	0.025 ± 0.012	
1992P	0.026	16.12	16.05 ± 0.02	1.060 ± 0.027	0.045 ± 0.018	0.020	0.009 ± 0.018	
1992ae	0.075	18.58	18.41 ± 0.04	0.957 ± 0.018	0.093 ± 0.028	0.036	0.003 ± 0.031	
1992ag	0.026	16.67	16.26 ± 0.02	1.053 ± 0.016	0.218 ± 0.021	0.097	0.186 ± 0.021	2,3
1992al	0.014	14.61	14.48 ± 0.01	0.959 ± 0.011	0.055 ± 0.013	0.034	0.025 ± 0.013	
1992aq	0.101	19.37	19.30 ± 0.04	0.876 ± 0.032	0.138 ± 0.028	0.012	0.022 ± 0.032	
1992bc	0.020	15.18	15.10 ± 0.01	1.053 ± 0.006	0.088 ± 0.009	0.022	0.047 ± 0.009	
1992bg	0.036	17.41	16.65 ± 0.04	1.002 ± 0.015	0.125 ± 0.027	0.181	0.010 ± 0.028	
1992bh	0.045	17.71	17.60 ± 0.02	1.026 ± 0.017	0.099 ± 0.018	0.022	0.097 ± 0.019	
1992bl	0.043	17.37	17.31 ± 0.03	0.813 ± 0.012	0.016 ± 0.023	0.012	0.005 ± 0.024	
1992bo	0.018	15.89	15.78 ± 0.01	0.756 ± 0.007	0.050 ± 0.012	0.027	0.060 ± 0.012	
1992bp	0.079	18.59	18.29 ± 0.01	0.905 ± 0.014	0.084 ± 0.015	0.068	0.059 ± 0.017	
1992br	0.088	19.53	19.38 ± 0.03	0.695 ± 0.023	0.194 ± 0.044	0.027	0.056 ± 0.049	1–3
1992bs	0.063	18.26	18.20 ± 0.04	1.035 ± 0.016	0.008 ± 0.023	0.013	0.035 ± 0.025	
1993B	0.071	18.74	18.38 ± 0.04	1.019 ± 0.019	0.178 ± 0.028	0.080	0.067 ± 0.030	
1993O	0.052	17.87	17.64 ± 0.01	0.926 ± 0.009	0.039 ± 0.012	0.053	0.016 ± 0.013	
1993ag	0.050	18.32	17.83 ± 0.02	0.935 ± 0.016	0.214 ± 0.020	0.111	0.118 ± 0.021	2,3
1994M	0.024	16.33	16.24 ± 0.03	0.882 ± 0.015	0.041 ± 0.023	0.023	0.064 ± 0.023	
1994S	0.016	14.85	14.78 ± 0.02	1.033 ± 0.026	0.061 ± 0.019	0.018	0.010 ± 0.019	
1995ac	0.049	17.23	17.05 ± 0.01	1.084 ± 0.013	0.022 ± 0.011	0.042	0.011 ± 0.012	
1995bd	0.016	17.34	15.32 ± 0.01	1.039 ± 0.008	0.734 ± 0.008	0.490	0.348 ± 0.008	1–3
1996C	0.030	16.62	16.56 ± 0.04	1.119 ± 0.022	0.009 ± 0.028	0.014	0.048 ± 0.029	
1996ab	0.125	19.72	19.56 ± 0.02	0.930 ± 0.029	0.171 ± 0.023	0.032	0.086 ± 0.027	
1996bl	0.035	17.08	16.67 ± 0.01	1.031 ± 0.015	0.090 ± 0.012	0.099	0.033 ± 0.012	
1996bo	0.016	16.18	15.85 ± 0.01	0.862 ± 0.006	0.405 ± 0.008	0.077	0.387 ± 0.008	1–3

a: Supernovae through 1993ag are from H96, later ones from R99.
b: This is the measured peak magnitude of the B-band lightcurve.
c: This value has been K-corrected and corrected for Galactic extinction.
d: This is the measured B-V color at the epoch of rest-frame B-band lightcurve maximum.
e: Schlegel, Finkbeiner, & Davis (1998)
f: These supernovae are excluded from the indicated subsets; § 2.5.

Table 6: U-B SN Ia Colors at Epoch of B-band Maximum

SN	Raw U-B^a	Corrected U-B^b	Reference
1980N	0.21	0.29	Hamuy *et al.* (1991)
1989B	0.08	0.33	Wells *et al.* (1994)
1990N	0.35	0.45	Lira *et al.* (1998)
1994D	0.50	0.52	Wu, Yan, & Zou (1995)
1998bu	0.23	0.51	Suntzeff *et al.* (1999)

a: This is the measured U-B value from the paper
b: This U-B value K-corrected, and corrected for host-galaxy and Galactic extinction

the data is not determinative (see Section 5.4 for the effect of systematic error in this value). Any intrinsic uncertainty in B-V is already subsummed within the assumed intrinsic dispersion of extinction-corrected peak magnitudes (see § 2.4); however, we might expect a larger dispersion in intrinsic U-B due to e.g., metallicity effects (Hoeflich, Wheeler, & Thielemann 1998; Lentz *et al.* 2000). The low-redshift U-band photometry may also have unmodeled scatter e.g., related to the lack of extensive UV supernova spectrophotometry for K-corrections. The effect on extinction-corrected magnitudes will be further increased by the greater effect of dust extinction on the bluer U-band light. The scatter of our extinction-corrected magnitudes about the best-fit cosmology suggests an intrinsic uncertainty in U-B of 0.04 magnitudes. This is also consistent with the U-B data of Jha (2002) over the range of timescale stretch of our $z > 0.6$ SNe Ia, after two extreme color outliers from Jha (2002) are removed; there is no evidence of such extreme color objects in our dataset. Note that this intrinsic U-B dispersion is in addition to the intrinsic magnitude dispersion assumed after extinction correction.

The template spectrum which has been constructed may be used to perform color- and K-corrections on both the low- and high-redshift supernovae to be used for cosmology. However, it must be further modified to account for the reddening effects of dust extinction in the supernova host galaxy, and extinction of the redshifted spectrum due to Galactic dust. To calculate the reddening effects of both Galactic and host-galaxy extinction, we used the interstellar extinction law of O'Donnell (1994) with the standard value of the parameter $R_V = 3.1$. Color excess ($E(B\text{-}V)$) values due to Galactic extinction were obtained from Schlegel, Finkbeiner, & Davis (1998).

The $E(B\text{-}V)$ values quoted in Tables 3, 4, and 5 are the values necessary to reproduce the observed R-I color at the epoch of the maximum of the rest-frame B lightcurve. This reproduction was performed by modifying the spectral template exactly as described above, given the intrinsic color of the supernova of the fit stretch, the Galactic extinction, and the host-galaxy $E(B\text{-}V)$ parameter. The modified spectrum was integrated through the Bessell R- and I-band filters, and $E(B\text{-}V)$ was varied until the R-I value matched the result from the lightcurve fit.

For each supernova, this finally modified spectral template was integrated through the Bessell and WFPC2 filter transmission functions to provide color and K-corrections. The exact spectral template needed for a given data point on a given supernova is dependent on parameters of the fit: the stretch, the time of each point relative to the epoch of rest-B maximum, and the host-galaxy $E(B\text{-}V)$ (measured as described above). Thus, color and K-corrections were performed iteratively with lightcurve fitting in order to generate the final corrections used in the fits described in § 2.2. An initial date of maximum, stretch, and host-galaxy extinction was assumed to generate K-corrections for the first iteration of the fit. The parameters resulting from that fit were used to generate new color and K-corrections, and the whole procedure was repeated until the results of the fit converged. Generally, the fit converged within 2–3 iterations.

2.4. Cosmological Fit Methodology

Cosmological fits to the luminosity distance modulus equation from the Friedmann-Robertson-

Walker metric followed the procedure of P99. The set of supernova redshifts (z) and K-corrected peak B-magnitudes (m_B) were fit to the equation

$$m_B = \mathcal{M} + 5\log\mathcal{D}_{\mathcal{L}}(z;\Omega_{\rm M},\Omega_\Lambda) \quad \alpha(s \quad 1) \quad (3)$$

where s is the stretch value for the supernova, $\mathcal{D}_{\mathcal{L}} \equiv H_0 d_L$ is the "Hubble-constant-free" luminosity distance (Perlmutter *et al.* 1997), and $\mathcal{M} \equiv M_B \quad 5\log H_0 + 25$ is the "Hubble-constant-free" B-band peak absolute magnitude of a $s = 1$ SN Ia with true absolute peak magnitude M_B. With this procedure, neither H_0 nor M_B need be known independently. The peak magnitude of a SN Ia is mildly dependent on the lightcurve decay time scale, such that supernovae with a slower decay (higher stretch) tend to be over-luminous, while supernovae with a faster decay (lower stretch) tend to be under-luminous (Phillips *et al.* 1993); α is a slope that parameterizes this relationship.

There are four parameters in the fit: the mass density $\Omega_{\rm M}$ and cosmological constant Ω_Λ, as well as the two nuisance parameters, $\mathcal{M}$ and α. The four-dimensional ($\Omega_{\rm M}$, Ω_Λ, $\mathcal{M}$, α) space is divided into a grid, and at each grid point a χ^2 value is calculated by fitting the luminosity distance equation to the peak B-band magnitudes and redshifts of the supernovae. The range of parameter space explored included $\Omega_{\rm M} = [0, 3)$, $\Omega_\Lambda = [\ \ 1, 3)$ (for fits where host-galaxy extinction corrections are not directly applied) or $\Omega_{\rm M} = [0, 4]$, $\Omega_\Lambda = [\ \ 1, 4)$ (for fits with host-galaxy extinction corrections). The two nuisance parameters are fit in the ranges $\alpha = [\ 1, 4)$ and $\mathcal{M} = [\ 3.9, 3.2)$. No further constraints are placed on the parameters. (These ranges for the four fit parameters contain $> 99.99\%$ of the probability.) At each point on the 4-dimensional grid, a χ^2 is calculated, and a probability is determined from $P \propto e^{\ \chi^2/2}$. The probability of the whole 4-dimensional grid is normalized, and then integrated over the two dimensions corresponding to the "nuisance" parameters.

For each fit, all peak m_B values were corrected for Galactic extinction using $E(B\text{-}V)$ values from Schlegel, Finkbeiner, & Davis (1998), using the extinction law of O'Donnell (1994) integrated through the *observed* filter.[29] For our primary fits, the total effective statistical uncertainty on each value of m_B included the following contributions:

- the uncertainty on m_B from the lightcurve fits;
- the uncertainty on s, multiplied by α
- the covariance between m_B and s;
- a contribution from the uncertainty in the redshift due to peculiar velocity (assumed to have a dispersion of 300 km s ^{1});
- 10% of the Galactic extinction correction; and
- 0.17 magnitudes of intrinsic dispersion (H96).

Fits where host-galaxy extinction corrections are explicitly applied, use the first five items above plus:

- the uncertainty on $E(B\text{-}V)$ multiplied by R_B;
- the covariance between $E(B\text{-}V)$ and m_B;
- 0.11 magnitudes of intrinsic dispersion (Phillips *et al.* 1999); and
- 0.04 magnitudes of intrinsic $U\text{-}B$ dispersion (see below).

Host-galaxy extinction corrections used a value $R_B \equiv A_B/E(B\text{-}V) = 4.1$, which results from passing a SN Ia spectrum through the standard O'Donnell (1994) extinction law. Except where explicitly noted below, the $E(B\text{-}V)$ uncertainties are *not* reduced by any prior assumptions on the intrinsic color excess distribution. Although there is almost certainly some intrinsic dispersion either in the proper value of R_B to use, or in the true $B\text{-}V$ color of a SN Ia (Nobili *et al.* 2003), we do not explicitly include such a term. The effects of such a dispersion is included, in principle, in the 0.11 magnitudes of intrinsic magnitude dispersion which Phillips *et al.* (1999) found after applying extinction corrections.

As discussed in § 2.3, the intrinsic $U\text{-}B$ dispersion is likely to be greater than the intrinsic $B\text{-}V$ dispersion. For those supernovae most affected by this (i.e. those at $z > 0.7$), we included an additional uncertainty in magnitude corresponding to 0.04 magnitudes of intrinsic $U\text{-}B$ dispersion, converted into a magnitude error using the O'Donnell extinction law.

This set of statistical uncertainties is slightly different from those used in P99. For these fits, the

[29] This supersedes P99, where an incorrect dependence on z of the effective R_R for Galactic extinction was applied. The corrected procedure decreases the flat-universe value of $\Omega_{\rm M}$ by 0.03.

test value of α was used to propagate the stretch errors into the corrected B-band magnitude errors; in contrast, P99 used a single value of $\alpha = 1.74$ for purposes of error propagation.

2.5. Supernova Subsets

In P99, separate analyses were performed and compared for the supernova sample before and after removing supernovae with less secure identification as Type Ia. The results were shown to be consistent, providing a cross-check of the cosmological conclusions. For this current analysis, the "complete set" combines the supernovae from the four samples: supernovae from H96 and R99 (matching the selection criteria in § 2.2) at low redshift, and P99 and the new supernovae in this paper at high redshift; only the 35 P99 high-redshift supernovae with color measurements are included in the complete set. For most of the analyses of this paper, adding and comparing eleven very-well-measured SNe Ia, we take the more securely identified SNe Ia as our primary subset. This further excludes four supernovae from P99 (SNe 1994G, 1995aq, 1995at, and 1997K) that are very likely to be SNe Ia, but without good spectral confirmation. Following P99, we omit one supernova which is an outlier in the stretch distribution, with $s < 0.7$ (SN 1992br), and one SN which is a $> 6\sigma$ outlier from the best-fit cosmology (SN 1997O). Finally, we omit those supernovae which are most seriously reddened, with $E(B\text{-}V) > 0.25$ and $> 3\sigma$ above zero; host-galaxy extinction corrections, even though they work well for objects of more mild reddening, ~~appear to overcorrect these most severely reddened objects~~ (Phillips *et al.* 1999). This cut removes an additional four supernovae, including two at low redshift and one of the eleven HST supernovae from this paper (SNe 1995bd, 1996bo, 1996cn, and 1998aw). The resulting "full primary subset" of SNe Ia, Subset 1, is further culled to remove likely reddened supernovae, producing a "low-extinction primary subset," Subset 2. This subset omits five supernovae with host-galaxy $E(B\text{-}V) > 0.1$ and $> 2\sigma$ above zero, including three of the HST supernovae from this paper (SNe 1992ag, 1993ag, 1998as, 1998ax, and 1998be). The low-extinction primary subset includes seven of the eleven new HST supernovae presented in this paper.

Subset 3, the "low-extinction strict Ia subset," makes an even more stringent cut on spectral confirmation, including only those supernovae whose confirmations as Type Ia SNe are unquestionable. This subset is used in § 5.2 to estimate any possible systematic bias resulting from type contamination. An additional five supernovae, including one of the HST supernovae from this paper, are omitted from Subset 3 beyond those omitted from Subset 2; these are SNe 1995as, 1996cf, 1996cg, 1996cm, and 1998ay.

3. Colors and Extinction

In this section, we discuss the limits on host-galaxy extinction we can set based on the measured colors of our supernovae. For the primary fit of our P99 analysis, extinction was estimated by comparing the mean host-galaxy $E(B\text{-}V)$ values from the low- and high-redshift samples. Although the uncertainties on individual $E(B\text{-}V)$ values for high-redshift supernovae were large, the uncertainty on the mean of the distribution was only 0.02 magnitudes. P99 showed that there was no significant difference in the mean host-galaxy reddening between the low and high-redshift samples of supernovae of the primary analysis (Fit C). This tightly constrained the systematic uncertainty on the cosmological results due to differences in extinction. Riess *et al.* (1998) did apply host-galaxy extinction corrections to each individual supernova, but used a Bayesian prior on the color-excess distribution to modify the extinction correction. This prior was one sided, with zero probability for $E(B\text{-}V) < 0$, and a probability which sharply falls for positive values of $E(B\text{-}V) > 0.02$ magnitudes, based on the models of Hatano, Branch, & Deaton (1998). Even if all $E(B\text{-}V)$ values are intrinsically close to zero, measurements will scatter to both sides of zero by an amount given by the measurement uncertainty; consequently, applying this asymmetric prior biases the measured $E(B\text{-}V)$ distribution to the red. A constant bias in supernova magnitudes will not affect measurements of $\Omega_{\rm M}$ and Ω_Λ (as those parameters are only sensitive to the *differences* in the magnitudes between high-redshift and low-redshift supernovae). However, if the uncertainties on the color excesses of the low- and high-redshift samples differ, then the offset resulting from this prior will differ and bias is introduced into the cosmology. ~~In P99, Fit E applies this one-sided extinction prior to the high-~~

Fit E of P99 and

As discussed in P99,

[Can this be said a little more simply, so that it doesn't start people thinking that the bias is due to the first reason and then have to correct the impression?]

have been found in studies of low-redshift supernovae to overcorrect these reddest objects

[For Saul and Greg to do: Reword this to explain how reddest could be due to other things besides ordinary extinction (perhaps intrinsic color or odd dust)?]

Start a new paragraph here.

[We need a paragraph around here to explain *why* the Hatano et al prior isn't a crazy one, if it is used more correctly -- and why we use it to suggest that it is useful to compare the low-extinction subset analysis to a full analysis. The reason Hatano et al prior isn't crazy is simply that the scale-height of stars (and in particular white dwarfs stars) is higher than that of dust in the disks of spirals,...)]

Table 7: Mean $E(B\text{-}V)$ Values

Sample	Complete Set	Low-extinction Primary Subset SNe[a]
Low z	$+0.107 \pm 0.003$	0.000 ± 0.004
P99	$+0.024 \pm 0.023$	$+0.002 \pm 0.025$
HST	$+0.094 \pm 0.012$	$+0.007 \pm 0.016$

a: SNe omitted from our low-extinction primary subset, Subset 2, (§ 2.5) have been omitted from these means. This excludes outliers, as well as supernovae with both $E(B\text{-}V) > 0.1$ and $E(B\text{-}V) > 2\sigma$ above zero.

[Should we put boxes around the points on this plot (or make them filled circles) that are cut out of the low-extinction sample?]

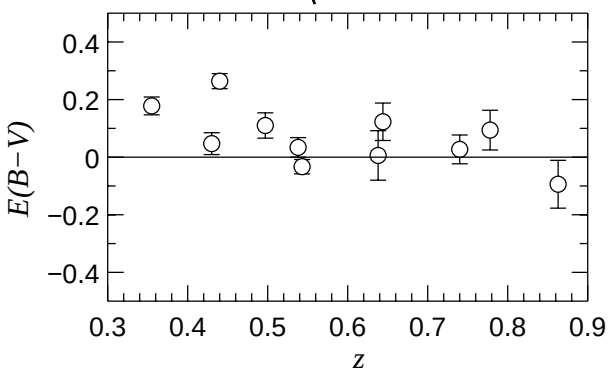

Fig. 4.— A plot of $E(B\text{-}V)$ as a function of redshift for the 11 HST-observed supernovae of this paper shows that the blue edge of the distribution shows no evolution with redshift. Error bars include only measurement errors, and no assumed intrinsic color dispersion.

~~redshift SCP data,~~ because of the bias introduced, P99 cautioned against this approach. The small dispersion of the prior makes the cosmological fits appear much better constrained by reducing the propagated $E(B\text{-}V)$ measurement uncertainties, especially for supernovae with $E(B\text{-}V) < 0$ (as was the case for more than half of those in Riess *et al.* (1998)). The effect this prior would have on the fits of this paper is discussed in § 4.1.

[italics?]

The high precision measurements of the $R\text{-}I$ color afforded by the WFPC2 lightcurves for the new supernovae in this work allow a direct estimation of the host-galaxy $E(B\text{-}V)$ color excess without any need to resort to a prior assumption concerning the intrinsic color-excess distribution.

Figure 3 shows histograms of the host-galaxy $E(B\text{-}V)$ values from different samples of supernovae. For the bottom two panels, a line is overplotted that treats the H96 $E(B\text{-}V)$ values as a parent distribution, and shows the expected distribution for the other samples given their measurement uncertainties. Each sample's distribution is ~~approximately~~ consistent with the $E(B\text{-}V)$ distribution from H96, except for R99 which shows a few significantly reddened supernovae. The R99 supernovae are not all from a flux-limited sample, and therefore are more likely to include extincted supernovae that would be selected against in flux-limited samples such as H96 and all high-redshift supernovae. Four of the eleven HST supernovae of this paper are significantly reddened (with $E(B\text{-}V) > 2\,\sigma$ above zero); three of these are at lower redshifts ($z < 0.5$).

[See comments written on Figure 3. Hopefully, these will result in each low-extinction sample's distribution being consistent, not "approximately consistent".]

Figure 4 shows $E(B\text{-}V)$ vs. z for the eleven supernovae of this paper. Three of the lowest redshift SNe are clearly reddened: SN 1998as at $z = 0.36$, SN 1998aw at $z = 0.44$, and SN 1998ax at $z = 0.50$; additionally, SN 1998be at $z = 0.64$ is reddened. That most of the reddened supernovae fall at the low end of the redshift range is as would be expected for a flux-limited survey. Several authors (including Leibundgut (2001) and Falco *et al.* (1999)) have used the Riess *et al.* (1998) $E(B\text{-}V)$ values to suggest that there is evidence that high-redshift supernovae are bluer statistically than the low-redshift counterparts they are compared with. These data show no such effect (nor did our P99 SNe).

[This sounds a little like they did something devious -- try a minor rewording.]

Table 7 lists the variance-weighted mean $E(B\text{-}V)$ values for the low-redshift supernoave and for each sample of high-redshift supernoave. Although varying amounts of extinction are detectable in the mean colors of each sample, the supernovae in the low-extinction primary subset (§ 2.5) of each samples are consistent with $E(B\text{-}V) = 0$. We will consider cosmological fits both to this low-extinction subset and to the primary subset with host-galaxy reddening corrections applied.

The mean host-galaxy color excess calculated for the highest redshift supernovae is critically dependent on the assumed intrinsic $U\text{-}B$ color (see Section 2.3). An offset in $U\text{-}B$ will af-

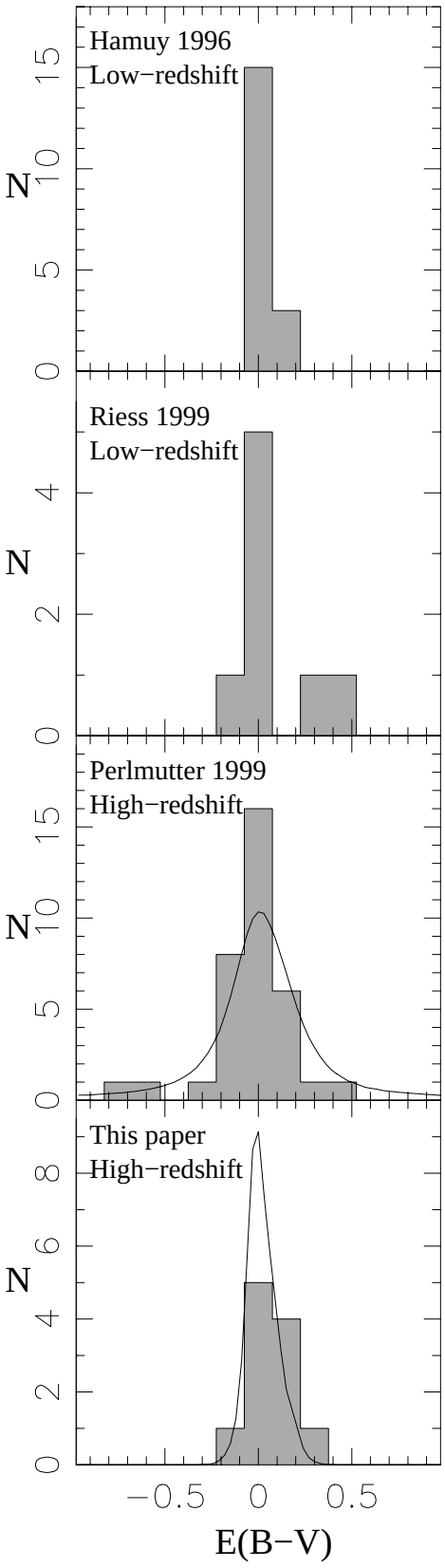

Two *important* things to fix with this figure now:1. What is the odd bin-size that is being used here? Can we use any bin-size that's less weird-looking?

2. Now that we are removing so many red SNe from the low-extinction set, the histograms should be filled in grey only for the low-extinction supernovae, and open outlines for the red SNe that are removed from the low-extinction subset.
Also, the solid line drawn over the bottom two panels should now only contain enough supernovae for the low-extinction SNe from each panel (and be drawn from the low-extinction set from the Hamuy top panel), so that it can test the hypothesis that the low-extinction samples are all consistent.

Fig. 3.— Histograms of $E(B\text{-}V)$ for the four samples of supernovae used in this paper. All supernovae with measured colors are plotted. The solid lines drawn over the bottom two panels is a simulation of the distribution expected if the H96 sample represented the true distribution of SN colors, given the error bars of each high-redshift sample.

[The "canceling" is no longer discussed above (is it?), so this is now harder to understand.]

fect the high-redshift supernovae much more than the low-redshift supernovae (whose measurements are primarily of the rest frame B- and V-band lightcurves), and thus there is no "canceling" effect in U-B as is discussed above for a slight offset in B-V. The K-corrected magnitudes are also dependent on the assumed supernova colors that went into deriving the K-corrections. If the assumed U-B color is too red, that will affect the cross-filter K-correction applied to R band data at $z \gtrsim 0.5$, thereby changing derived rest frame colors. In § 5, we consider the effect of changing the reference U-B color.

4. Cosmological Results

4.1. $\Omega_{\rm M}$ and Ω_Λ

Figures 5 and 6 show Hubble Diagrams which plot K-corrected rest-frame B-band peak magnitudes and redshifts for the new supernovae of this paper. Figure 5 show all of the data in the full set of supernovae. Figure 6 show just the eleven HST supernovae from this paper. In the upper panel of this latter figure, the m_B values and uncertainties from Table 3 are plotted. In the lower panel, m_B values have been corrected for host-galaxy extinction based on measured $E(B\text{-}V)$ values. The most reddened supernova— SN 1998aw at $z = 0.44$— is overcorrected by the extinction correction, and falls 3σ below the best-fit cosmology. Phillips *et al.* (1999) found that to best correct host-galaxy extinction for low-redshift SNe Ia, one needs a value of R_B which is slightly lower than the standard value; these high-redshift supernovae would seem to support that conclusion. The effect of changing this value will be considered as a systematic in § 5.5.

Table 8 lists results from fits to our full set of supernovae and to both of our primary subsets. The first three lines show fits to the low-extinction primary subset. So that the new sample of high-redshift supernovae may be compared to those from P99, separate fits have been performed using only the high-redshift supernovae from each sample. Fit 3 combines all of the current SCP high-redshift supernovae, and represents the primary result for this paper. Fits 4–6 show the fits to the primary subset when host-galaxy extinction corrections have been applied. Finally, for comparison purposes, Fits 7–8 show fits to the complete set of supernovae.

[Hmm... I don't think we should go into this again here -- that was the whole point of cutting this one out of the primary subset and explaining it there! (And I think also these SNe not in the primary subset should be greyed out of Figure 5, and then maybe even removed from Fig 6??)]

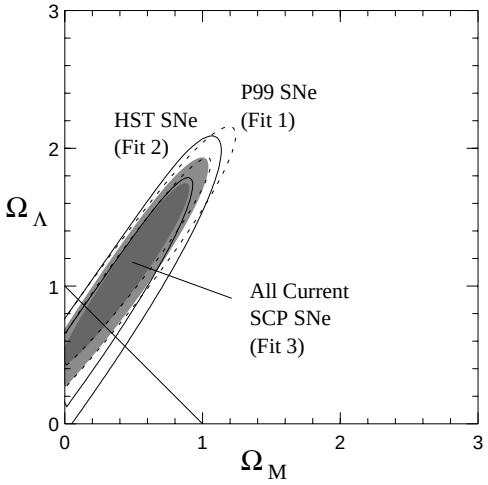

Fig. 8.— Contours indicate 68% and 90% confidence regions for fits to supernovae from the low-extinction primary subset, including just the high-redshift SNe from P99 (dotted lines), just the new HST high-redshift SNe (solid lines), and all SCP high-redshift SNe (filled contours). The low-redshift SNe from the primary subset are included in all fits. The new, independent sample of high-redshift supernovae provide measurements of $\Omega_{\rm M}$ and Ω_Λ consistent with those from the previous sample.

Figure 7 shows the confidence regions for $\Omega_{\rm M}$ vs. Ω_Λ from our current primary fit (Fit 3 in Table 8), which includes the low-extinction primary subset (Subset 2) high-redshift supernovae both from P99 and from this work. Figure 8 shows the comparison of the confidence regions when each high-redshift sample is treated separately; several parameters from these fits are tabulated in Table 8 (Fits 1–3). Note that Fit 2 provides comparable and consistent measurements of $\Omega_{\rm M}$ and Ω_Λ to Fit 1. Additionally, the size of the confidence regions from the 7 HST SNe in Fit 2 is similar to those in Fit 1, which includes 27 high-redshift supernovae from P99.

Figure 9 compares these results to the cosmological fits for the full primary subset with host-galaxy extinction corrections applied (Fits 4–6 in

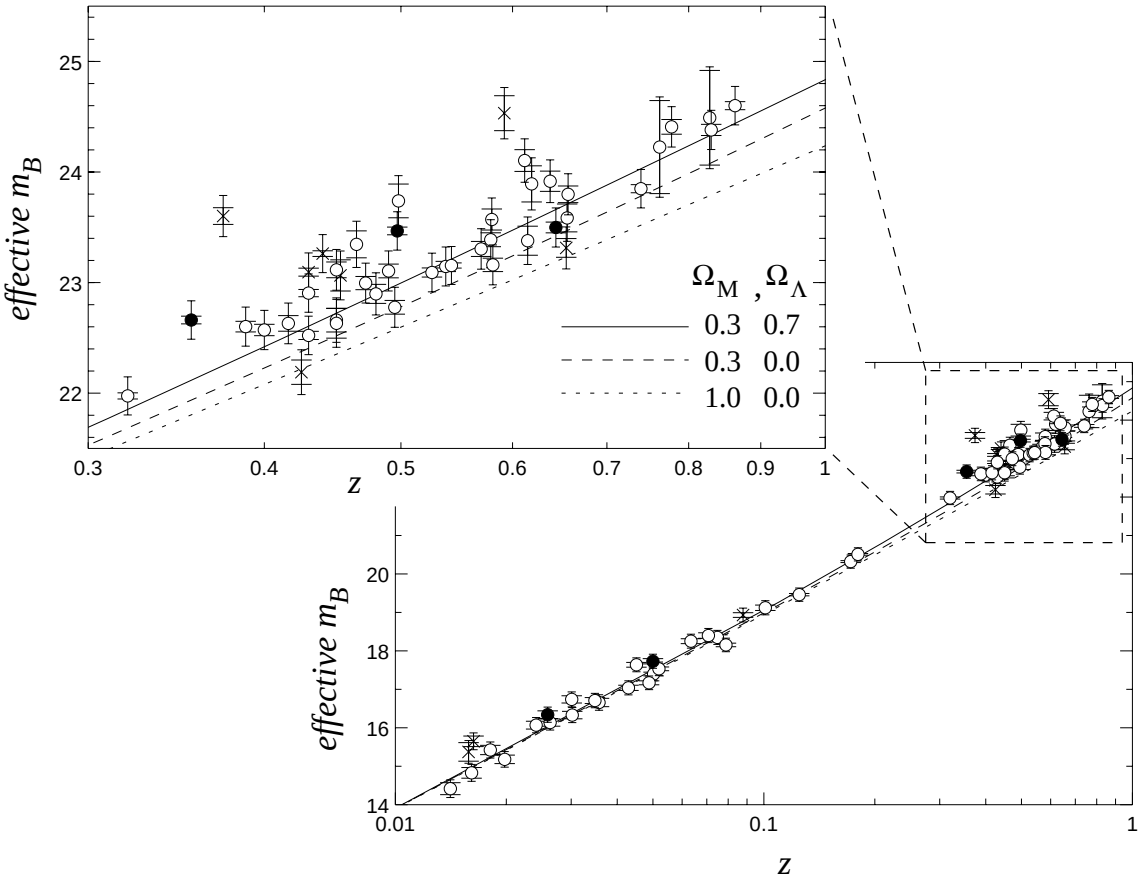

Fig. 5.— Hubble diagram of effective m_B vs. redshift for all of the supernovae in the full set of this paper. Points plotted as crosses are omitted from all primary subsets. Circles represent points in the primary subset (Subset 1); filled circles are omitted from the low-extinction primary subset (Subset 2). Inner error bars show just the measurement uncertainties; outer error bars include 0.17 magnitudes of intrinsic dispersion.

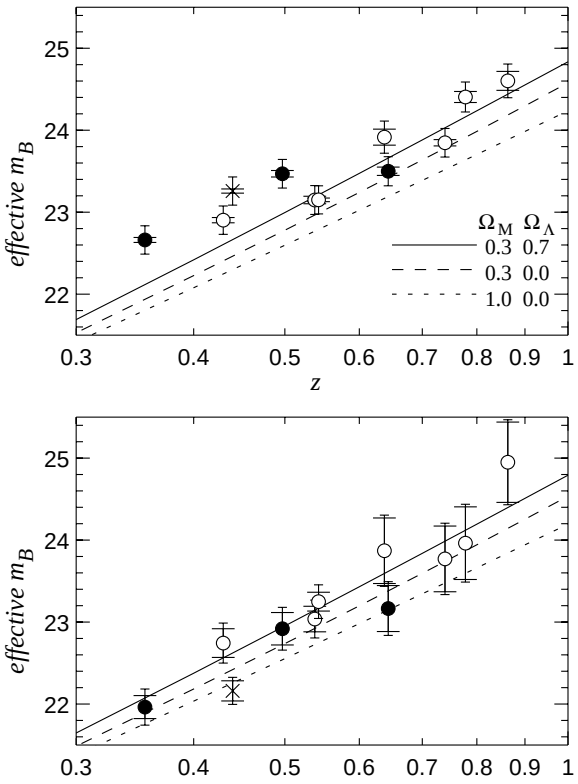

Fig. 6.— Hubble diagram of effective m_B vs. redshift for the 11 supernovae observed with WFPC2 and reported in this paper. Circles represent supernovae in the primary subset (Subset 1); the one point plotted as a cross (SN 1998aw) is omitted from that subset. Filled circles represent reddened supernovae omitted from the low-extinction primary subset (Subset 2), while open circles are in both Subsets 1 and 2. In the upper plot, no host-galaxy $E(B\text{-}V)$ extinction corrections have been applied. Inner error bars only include the measurement error. Outer error bars include 0.17 magnitudes of intrinsic dispersion. In the lower plot, extinction corrections have been applied using the standard interstellar extinction law. Error bars have been increased by the uncertainty in this extinction correction. Again, inner error bars represent only measurement uncertainties, while outer error bars include 0.11 magnitudes of intrinsic dispersion. Lines are for three different model cosmologies with the indicated values of Ω_M and Ω_Λ.

Table 8: Cosmological fits

Fit #	High-Redshift SNe Included in Fit[b]	N_{SNe}	Min. χ^2/dof	Ω_M for Flat[b]	Ω_Λ for Flat[b]	$P(\Omega_\Lambda > 0)$	$\mathcal{M}$	α
Fits to the Low-Extinction Primary Subset								
1	P99	50	1.29	$0.21^{+0.07}_{0.07}$	$0.79^{+0.07}_{0.07}$	0.9999	3.49 ± 0.05	1.42 ± 0.32
2	New HST SNe from this paper	28	1.27	$0.25^{+0.09}_{0.08}$	$0.75^{+0.08}_{0.09}$	0.9935	3.47 ± 0.05	1.09 ± 0.40
3	**All SCP SNe**	**57**	**1.26**	$\mathbf{0.22^{+0.06}_{0.06}}$	$\mathbf{0.78^{+0.06}_{0.06}}$	**0.9999**	$\mathbf{3.48 \pm 0.05}$	$\mathbf{1.37 \pm 0.31}$
Fits to Full Primary Subset, with Extinction Correction								
4	P99	52	0.96	$0.16^{+0.18}_{0.14}$	$0.84^{+0.14}_{0.18}$	0.9953	3.55 ± 0.05	1.15±0.33
5	New HST SNe from this paper	33	1.05	$0.30^{+0.13}_{0.12}$	$0.70^{+0.12}_{0.13}$	0.9888	3.54 ± 0.06	1.09±0.31
6	All SCP SNe	62	0.95	$0.28^{+0.12}_{0.10}$	$0.72^{+0.10}_{0.12}$	0.9943	3.53 ± 0.05	0.97±0.30
Fit to the Complete Set, No Extinction Correction								
7	All SCP SNe	72	2.41	$0.26^{+0.06}_{0.06}$	$0.74^{+0.06}_{0.06}$	0.9999	3.45 ± 0.04	1.81±0.27
Fit to the Complete Set, With Extinction Correction								
8	All SCP SNe	72	1.51	$0.28^{+0.11}_{0.10}$	$0.72^{+0.10}_{0.11}$	0.9971	3.59 ± 0.05	0.87±0.29

a: All fits include the low-redshift SNe from H96 and R99. See § 2.5 for the definitions of the supernova subsets.
b: This is the intersection of the fit probability distribution with the line $\Omega_M + \Omega_\Lambda = 1$.

[Add this to make it clearer that these aren't just the P99 results.]

[I think I'm inclined to discuss these fits (here called "7" and "8") in the text, but not include them in the table.]

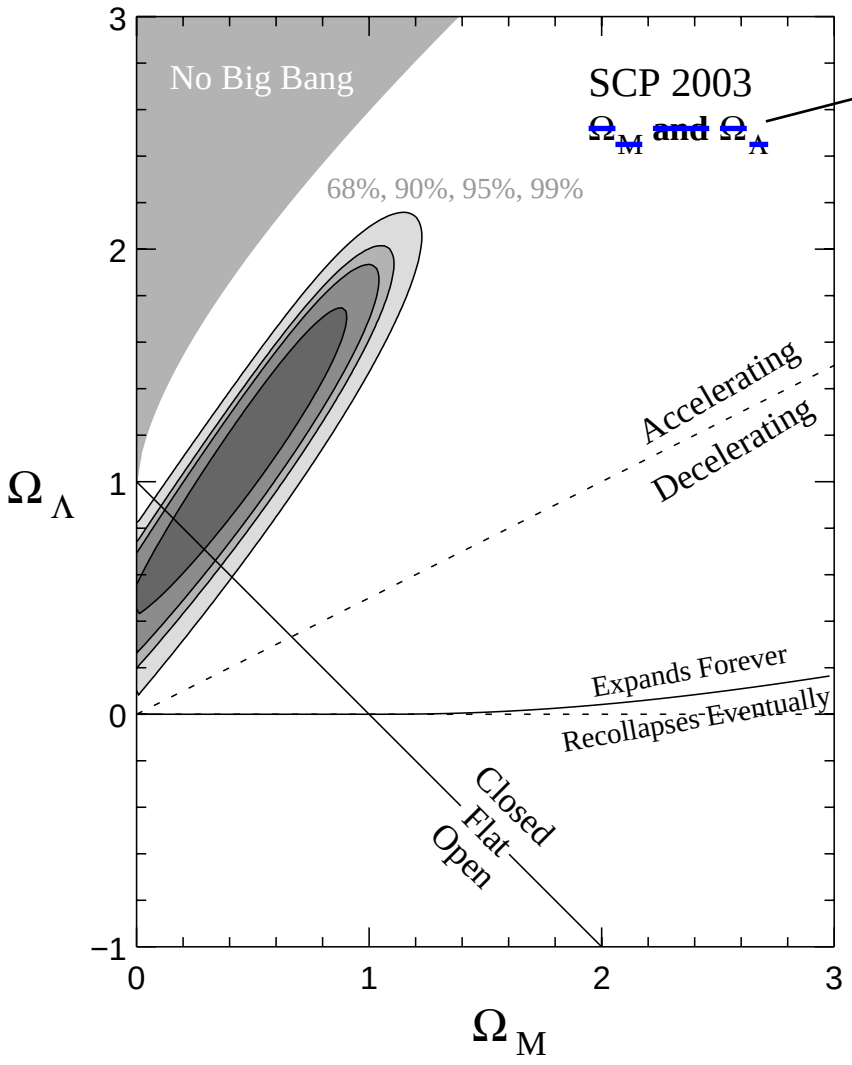

[I think this label should be cut, since it just repeats the axes, and doesn't really explain anything.]

Fig. 7.— Primary 68%, 90%, 95%, and 99% confidence regions for Ω_M and Ω_Λ from a fit to the low-extinction primary subset (Fit 3).

Table 8). The top row of this figure are the same primary fits plotted in Figure 8. The second row has $E(B\text{-}V)$ host-galaxy extinction corrections applied using the one-sided prior used by Fit E of P99 and Riess *et al.* (1998) discussed in § 3; because of bias introduced by this prior, we do not recommend using these results (see also appendix of P99). The third row has full extinction corrections applied without any prior assumptions on the intrinsic $E(B\text{-}V)$ distribution. Three conclusions are apparent from this plot. First, using a prior does, as expected, greatly reduce the apparent $E(B\text{-}V)$ error bars and hence apparently tightens the constraints of the cosmological confidence regions, but at the expense of biasing the results. Second, the current set of supernovae provide much smaller confidence regions on the Ω_Λ versus Ω_M plane than do the SNe Ia from previous high-redshift samples when unbiased extinction corrections are applied. Whereas Figure 8 shows that the current set of supernovae give comparable measurements of Ω_M and Ω_Λ when the low-extinction subsample is used with no host-galaxy extinction corrections, Figure 9 shows that the much higher precision color measurements from the WFPC2 data allows us directly to set much better limits on the effects of host-galaxy extinction on the cosmological results. Finally, the cosmology which results from the extinction-corrected fits is consistent with the fits to our low-extinction primary subset. Contrary to the assertion of Rowan-Robinson (2002), even when host-galaxy extinction is directly and fully accounted for in an unbiased manner, dark energy is still required, with $P(\Omega_\Lambda > 0) = 0.99$.

4.2. Combined High-Redshift Supernova Measurements

Figure 10 shows measurements of Ω_M and Ω_Λ which combine the high-redshift supernova data of Riess *et al.* (1998) together with the SCP data presented in this paper and in P99. The contours show confidence intervals from the 54 supernovae of the low-extinction primary Subset 2 (used in Fit 3 of Table 8), plus the nine well-observed confirmed Type Ia supernovae from Riess *et al.* (1998) (using the lightcurve parameters resulting from their template-fitting analysis); following the criteria of Subset 2, SN 1997ck from that paper has been omitted, as that supernova does not have a confirmimg spectral type identification. We also omit from Riess *et al.* (1998) the supernovae they measured using the "snapshot" method (which also lack a lightcurve color, but rather estimate extinction from the spectrum), and two SCP supernovae that Riess *et al.* (1998) used from the P99 data set. This fit has a minimum χ^2 of 73 with 63 supernovae. Under the assumption of a flat universe, it yields a measurement of the mass density of $\Omega_M = 0.24 \pm 0.06$, or equivalently a cosmological constant of $\Omega_\Lambda = 0.76 \pm 0.06$. Note that in this fit, the nine supernovae from Riess *et al.* (1998) were not treated in exactly the same manner as the others. The details of the template fitting will naturally have been different, which can introduce small differences (see § 5.1). More importantly, the K-corrections applied by the Riess *et al.* (1998) team to derive distance moduli were almost certainly different from those used in this paper.

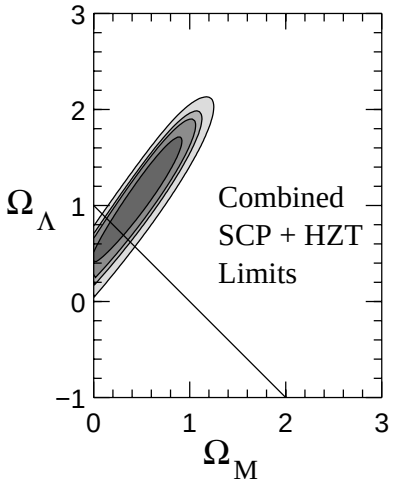

Fig. 10.— Ω_M and Ω_Λ 68%, 90%, 95%, and 99% confidence regions which combine the high-redshift data of the SCP (this paper and P99) and Riess *et al.* (1998). The fit includes Subset 2 supernovae from the SCP plus the nine well-observed confirmed SNe Ia from Riess *et al.* (1998).

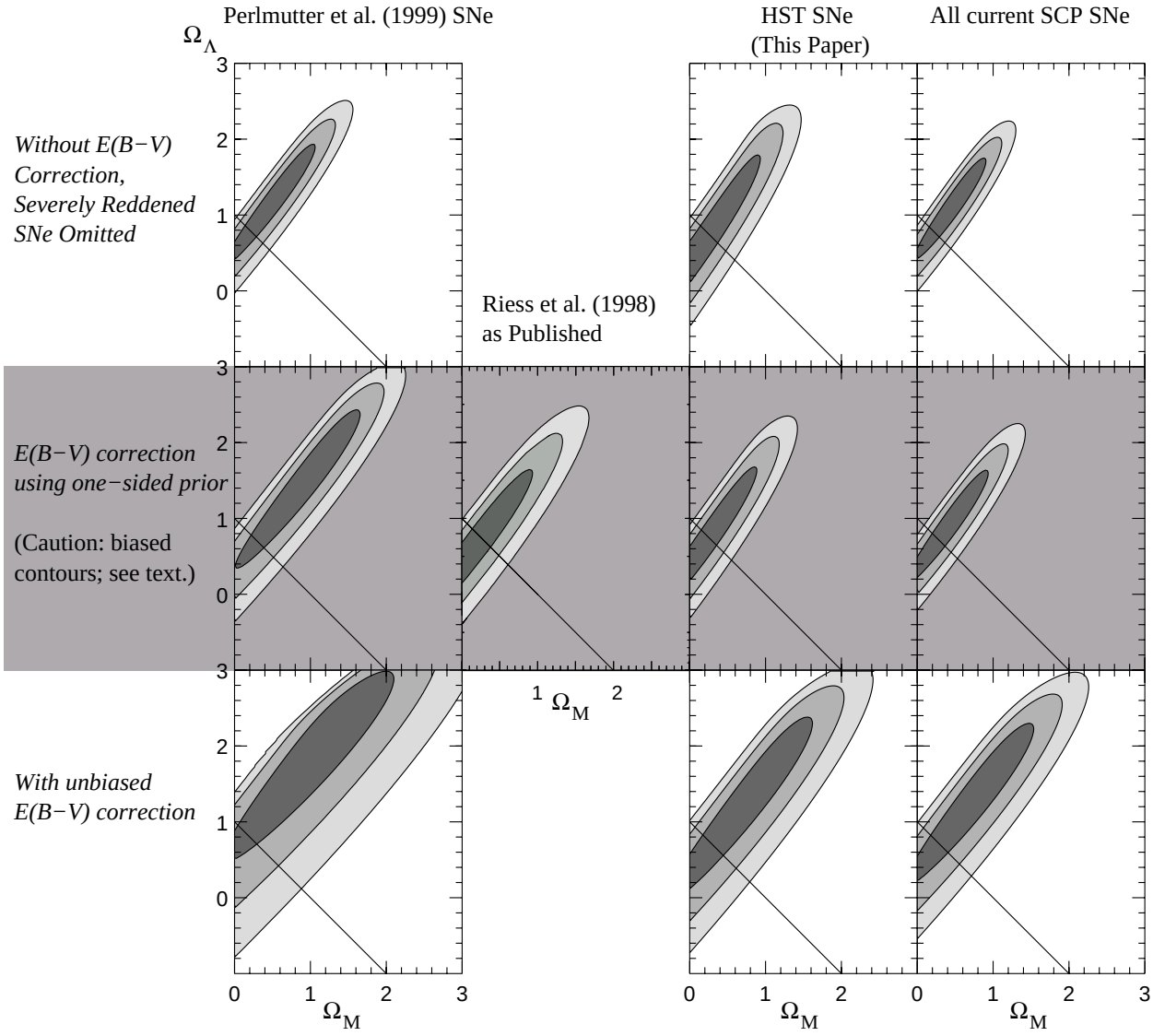

Fig. 9.— 68.3%, 95.4%, and 99.7% confidence regions for Ω_M and Ω_Λ using different data subsets and methods for treating host-galaxy extinction corrections. The top row represent our fits to the low-extinction primary subset, where significantly reddened supernovae have been omitted and host-galaxy extinction corrections are not applied. The second row shows fits where extinction corrections have been applied using a one-sided color-excess prior; this approach introduces bias and is not recommended (see text). Note that the published contours from Riess *et al.* (1998) in this row are the non-dashed contours from their Fig. 6, and result from fits that included not only well-observed supernovae, but also supernovae without lightcurve color measurements (the equivalents to which have been omitted from the SCP sets plotted in other panels), one supernova at $z = 0.97$ without a spectral confirmation, as well as two supernovae from the P99 set. The third row shows fits with unbiased extinction corrections applied to our primary subset. Comparisons of the different subsets of data show that the prior can improve the apparent precision of the fit cosmology, but that it introduces a bias which decreases the accuracy of the results. The HST SNe presented in this paper show a marked improvement in the precision of the color measurements, and hence in the precision of the Ω_M and Ω_Λ measurements when a full extinction correction is applied. With full and unbiased extinction corrections, dark energy is still required with $P(\Omega_\Lambda > 0) = 0.99$.

4.3. Dark Energy Equation of State

The fits of the previous section used a traditional constrained cosmology where $\Omega_{\rm M}$ is the energy density of non-relativistic matter (i.e. pressure $p = 0$), and Ω_Λ is the energy density in a cosmological constant (i.e. pressure $p = -\rho$, where ρ is the energy density). In Einstein's field equations, the gravitational effect enters in terms of $\rho + 3p$. If $w \equiv p/\rho$ is the equation of state parameter, then for matter $w = 0$, while for vacuum energy (i.e. a cosmological constant) $w = -1$. In fact, it is possible to achieve an accelerating Universe so long as there is a component with $w <\sim -1/2$. (If there were no contribution from $\Omega_{\rm M}$, only $w < -1/3$ dark energy is necessary for acceleration; however, for plausible mass densities $\Omega_{\rm M} \gtrsim 0.2$, the dark energy must have a more negative value of w.) The Hubble diagram for high-redshift supernovae provides measurements of w (P99, Garnavich *et al.* 1998b). The top two panels of Figure 11 show the joint confidence regions for $\Omega_{\rm M}$ versus w from the SCP supernovae, including the eleven new HST supernovae, under the assumptions that w is constant with time, and that the Universe is flat, i.e. $\Omega_{\rm M} + \Omega_X = 1$ (where Ω_X is the energy density in the component with equation of state w, in units of the critical density). By itself, the supernova data sets a 99% confidence limit of $w < -0.67$ for any positive value of $\Omega_{\rm M}$, without any prior assumptions on w. (When a fit with extinction corrections applied to the full primary subset gives a 99% confidence limit for $w < -0.86$.) However, w is not well bounded from below with the supernova data alone; although Figure 11 only shows confidence intervals down to $w = -2$, the 68% confidence interval from Fit 3 extends to $w < -4$, and the 99% confidence interval extends down to $w < -10$.

[Would it make more sense to use 90% or 95% conf limit, rather than 99%? NB: 95% would be consistant with what is used 3 paragraphs below]

Other methods provide measurements of $\Omega_{\rm M}$ and w which are complementary to the supernova results. Two of these measurements are plotted in the middle row of Figure 11, compared with the supernova measurements (in solid contours). In filled contours are results from the redshift-distortion parameter and bias-factor measurement of the 2dF Galaxy Redshift Survey (2dFGRS) (Hawkins *et al.* 2002; Verde *et al.* 2002). These provide a measurement of the the growth parameter, $f = 0.43 \pm 0.11$, at the survey redshift $z = 0.15$. We have used the method of Linder & Jenkins (2003) to directly solve for $f(\Omega_{\rm M}, w, z)$ rather than convert f to $\Omega_{\rm M}$, as the conversion formula given in Hawkins *et al.* (2002) is valid only for $w = -1$. Comparison of the 2dFGRS value of f with the calculated values of $f(\Omega_{\rm M}, w, z)$ yields the joint confidence region for $\Omega_{\rm M}$ and w.

In solid lines on the middle row of Figure 11 are contours representing confidence regions based on the distance to the surface of last scattering at $z = 1089$ from the Wilkinson Microwave Anisotropy Probe (WMAP) (Bennett *et al.* 2003; Spergel *et al.* 2003). For a given $\Omega_{\rm M}$ and w, this distance reduced distance to the surface of last scattering, I, is given by:

$$I = \int_0^{1089} [((1 - \Omega_{\rm M})/\Omega_{\rm M})(1+z)^{3(1+w)} + (1+z)^3]^{-1/2}\, dz \quad (4)$$

The plotted CMB constraints come from the "WMAPext" sample, which includes other CMB experiments in addition to WMAP; for $w = -1$, they yield a measurement of $I_0 = 1.76 \pm 0.058$, corresponding to $\Omega_{\rm M} = 0.29$. Confidence intervals are generated by calculating a $\chi^2 = [(I - I_0)/\sigma_{I_0}]^2$, where I is calculated for each $\Omega_{\rm M}, w$.

As both of these measurements show correlations between $\Omega_{\rm M}$ and w in a different sense from that of the supernova measurement, the combined measurements provide much tighter overall constraints on both parameters. The confidence regions which combine these three measurements are shown on the bottom row of Figure 11. When the resulting probability distribution is marginalized over $\Omega_{\rm M}$, we obtain a measurement of $w = -1.06^{+0.14}_{0.18}$ (for the low-extinction subset), or $w = -0.98^{+0.18}_{0.22}$ (for the full primary subset with host-galaxy extinction corrections applied). The 95% confidence limits on w when our data is combined with WMAP and 2dFGRS are $-1.53 < w < -0.79$ for the low-extinction primary subset, or $-1.51 < w < -0.61$ for the full extinction-corrected primary subset. If we add an additional prior that $w \geq -1$, we obtain a 95% upper confidence limit of $w < -0.80$ for the low-extinction primary subset, or $w < -0.65$ for the extinction-corrected full primary subset. These values may be compared with the limit in Spergel *et al.* (2003) which combines the CMB, 2dFGRS power spectrum, and HST key project

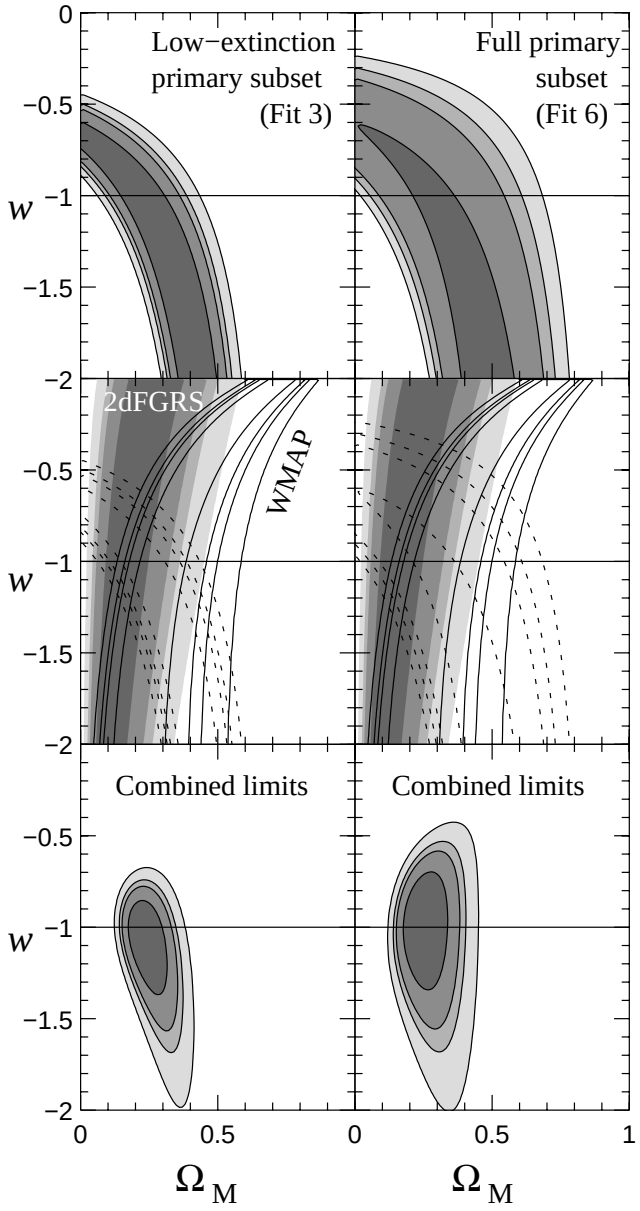

Fig. 11.— Joint measurements of $\Omega_{\rm M}$ and w assuming $\Omega_{\rm M} + \Omega_X = 1$ and that w is not time-varying. Confidence regions plotted are 68%, 90%, 95%, and 99%. The left column shows fits to the primary subset; the right column shows fits to the primary subset with unbiased individual host-galaxy extinction corrections applied to each supernova. The upper panels show the confidence intervals from the SCP supernovae alone. The middle panels overlay this (solid lines) with measurements from 2dFGRS (filled contours) (Hawkins *et al.* 2002) and WMAP (dotted contours) (Bennett *et al.* 2003; Spergel *et al.* 2003). The bottom plot combines the three data sets to provide a combined measurement of $\Omega_{\rm M}$ and w.

H_0 measurements to yield a 95% upper limit of $w < -0.78$. Although both our measurement and that of Spergel *et al.* (2003) include CMB data, they are complementary in that our limit does not include the H_0 prior, nor does it include any of the same external constraints, such as those from large scale structure.

These combined measurements remain consistent with a low density universe dominated by vacuum energy (constant $w = -1$), but also remain consistent with a wide range of other both time-varying-w and constant-w dark energy models.

5. Systematic Errors

The effect of most systematic errors in the Ω_M vs. Ω_Λ plane is asymmetric in a manner similar to the asymmetry of our statistical errors. For the effects listed below, a systematic difference will tend to move the confidence ellipses primarily along their major axis. In other words, for total identified systematic effects we have a larger uncertainty in $\Omega_M + \Omega_\Lambda$ than in $\Omega_M - \Omega_\Lambda$ (or, equivalently, in a measurement of Ω_M or Ω_Λ alone under the assumption of a flat universe). This means that systematic effects do not currently hamper the cosmological measurements from supernovae where they have the greatest weight relative to other techniques, nor do they significantly diminish the direct evidence from supernovae for the presence of dark energy. However, they do limit the ability of supernovae to measure the spatial curvature ("geometry") of the Universe. (Note that the semi-major axis is not precisely in the direction of $\Omega_M + \Omega_\Lambda$, nor is the semi-minor axis precisely aligned with $\Omega_M - \Omega_\Lambda$, but since these are useful constraints we will quantify the systematic uncertainties along these two directions.) Figure 12 shows the effects of some of the systematics discussed in the following subsections.

Systematic effects on flat-universe measurements of w are smaller than the current statistical uncertainties. The right column of Figure 12 shows the effect of the systematics on the Ω_M versus w confidence regions derived from our supernova data alone. To quantify the effect of identified systematics in the following subsections, we determine the shift in the maximum-likelihood value of w when the supernova data is combined with the Ω_M versus w confidence regions from 2dFGRS and WMAP (See § 4.3.)

5.1. Fit Method

There are multiple reasonable choices for lightcurve fitting methods which yield slightly different results for the lightcurve parameters. For the supernovae in P99, the R-band data on high-redshift supernovae provided much stronger limits on the stretch (the shape of the lightcurve) than did more sparse I-band lightcurves. For consistency, in P99 the stretch values for the low-redshift supernovae were therefore measured using only the B-band lightcurves.

In this paper, there are high-quality photometric measurements from WFPC2 in both R and I bands. Thus, data in both colors contribute significantly to the constraints on stretch. Additionally, the low background of the HST images, combined with the need to have previously subtracted the host-galaxy background in order to combine HST and ground-based data, indicate that it is more appropriate to fit these supernovae with fixed rather than floating lightcurve zero offsets. As this is the most appropriate fit method for the HST data, the low-redshift supernovae should be treated consistently. These procedures which are most appropriate for the HST supernovae were used for all new fits performed in this paper, and listed in Tables 3 through 5.

To estimate the size of the effect due to these differences in fitting method, cosmological confidence intervals were generated from the "Case C" subset of P99 using the new fits presented in this paper and compared to the results quoted in P99 and other variations on the fitting method. Differences in the fit method can change the flat-universe value of Ω_M by $\sim$0.03, and the value of $\Omega_M + \Omega_\Lambda$ by up to $\sim$0.8. (This is still much less than the major-axis extent of the statistical confidence ellipse in this direction.) We use these values as "fit-method" systematic uncertainties. We similarly performed joint fits to Ω_M, w in the flat-universe, constant-w case to the supernovae from P99 with different lightcurve fit methodologies, and from these fits adopt a fit-method systematic uncertainty of 0.02 on constant w (once combined with measurements from 2dFGRS and WMAP).

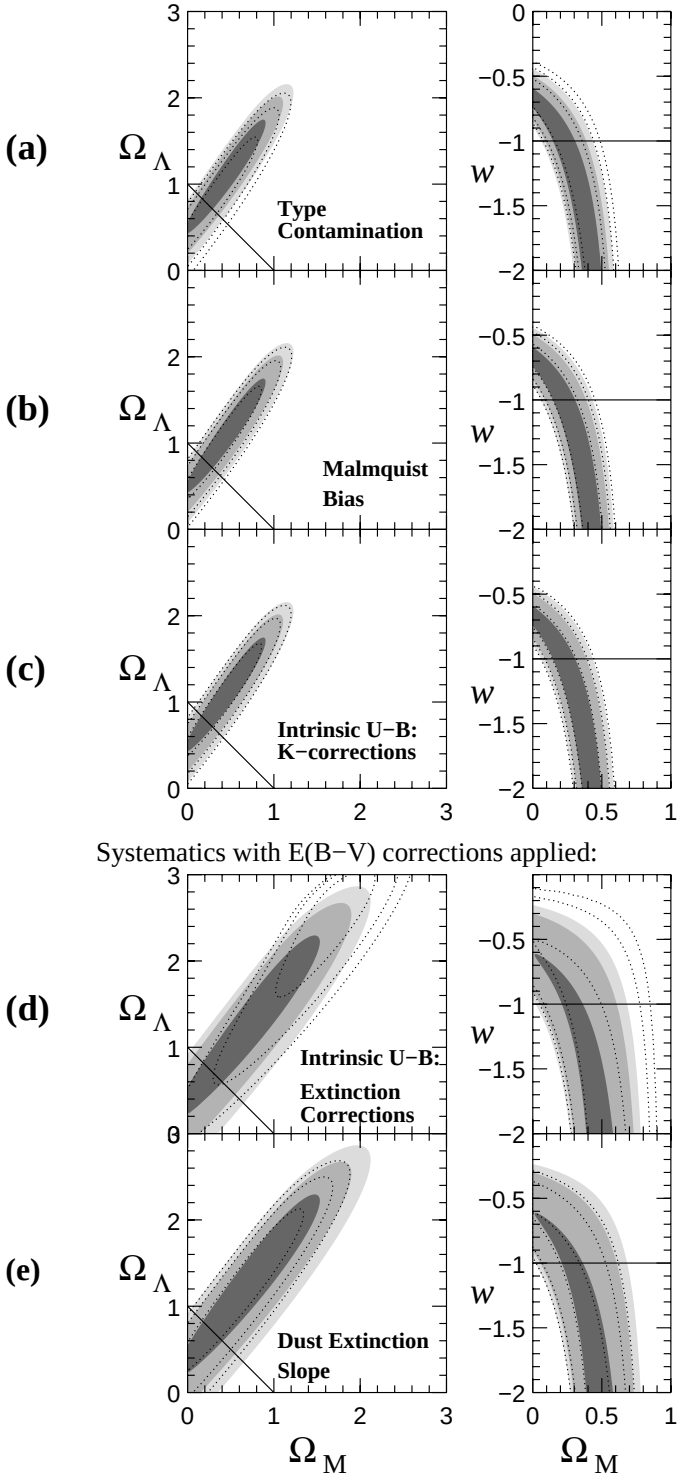

Fig. 12.— Simulated effects of identified systematic errors on the cosmological parameters, estimated by applying the systematic effect to the supernova parameters used in the cosmological fits. The left column shows fits to $\Omega_{\rm M}$ and Ω_Λ, and the right column to $\Omega_{\rm M}$ and the dark energy equation of state parameter w. Rows (a)–(d) show our standard fit (Fit 3) in filled contours. (a) The dotted contours show the results of a fit to Subset 3, only those supernovae with the most secure spectral identifications as Type Ia SNe. (b) The dotted contours show a fit to Subset 1 where the supernova magnitudes have been dimmed to correct for Malmquist bias. (c) The dotted contours show a fit to Subset 2, where K-corrections have been applied using a template spectrum with an intrinsic value of U-B= 0.5 at the epoch of B-maximum. (d) The filled contours is Fit 6, our standard fit with host-galaxy extinction corrections applied; the dotted contours show a fit to the same Subset, but using a template spectrum with an intrinsic value of U-B= 0.5 for estimating both K-corrections and color excesses. (e) The dotted contours apply extinction corrections to Subset 1 using a value of $R_B = 3.5$ rather than the standard $R_B = 4.1$ which was used for Fit 6 (filled contours).

5.2. Supernova Type Contamination

All subsets of supernovae used for cosmological fits in this paper omit supernovae for which there is not a spectral confirmation of the supernova type. Nonetheless, it is possible in some cases where that confirmation is weak that we may have contamination from non-Type Ia supernovae. To estimate such an effect, we performed fits using only those supernovae which have a firm identification as Type Ia; this is the "strict-Ia subset" from § 2.5. The comparison between our primary fit (Fit 3) and this fit with a more stringent type cut is shown in row (a) of Figure 12. This fit has a value of $\Omega_{\rm M}$ in a flat universe which is 0.03 higher than that of Fit 3. The value of $\Omega_{\rm M} + \Omega_\Lambda$ is 0.42 lower than that of Fit 3. We adopt these values as our "type contamination" systematic error.

The effect of changing our supernova subset on w is shown in the right panel of Figure 12a. Combined with WMAP and 2dFGRS, the best-fit value of w gets larger by 0.06; we adopt this as our type contamination systematic error on w.

5.3. Malmquist Bias

As most of our supernovae are from flux-limited samples, they will suffer Malmquist bias (Malmquist 1924, 1936). This effect was discussed extensively in P99, and here we update that discussion to include our new HST SNe Ia. For the measurement of the cosmological parameters, it is the difference between the Malmquist bias of the low-redshift and high-redshift samples which matters. In particular, the apparent probability of $\Omega_\Lambda > 0$ is enhanced only if the low-redshift supernovae suffer more Malmquist bias than the high-redshift supernovae, as this makes the high-redshift SNe Ia seem fainter.

The P99 high-redshift dataset was estimated to have little Malmquist bias (0.01 mag) because the SN discovery magnitudes were decorrelated with the measured peak magnitudes. However, for the new HST sample, nine of the eleven SNe Ia selected from full-search samples were found almost exactly at maximum light. This may reflect a spectroscopic flux limit superimposed on the original search flux limit since only spectroscopically confirmed SNe Ia were considered, and of those, generally the higher redshift SNe Ia from a given search were chosen for HST for follow-up. In particular, the SNe Ia selected for follow-up from the fall 1997 search were all found at maximum light, while all but SN 1998aw from the spring 1998 search were found at maximum light. SN 2000fr was found well before maximum. Thus, the new high-redshift dataset is likely to suffer more Malmquist bias than the P99 dataset. Further complicating the interpretation for the high-redshift supernovae is the fact that our new HST supernovae are spread over a wide range in redshift, such that a single brightness correction for Malmquist bias causes a more complicated change in the fitted cosmological parameters. This is unlike the situation in P99 in which most supernovae were at $z \sim 0.5$. Following the calculation in P99 for a high-redshift flux-limited SN sample we estimate that the maximum Malmquist bias for the ensemble of HST supernovae is ~ 0.03 mag. However, we caution that it is supernovae near the flux limit which are most strongly biased, and therefore, that a subsample comprised of the highest-redshift members drawn from a larger flux-limited sample will be more biased. When combined with the P99 high-redshift supernovae, the bias is likely to be ~ 0.02 mag since both samples have roughly the same statistical weight.

As for the low-redshift SNe Ia, in P99 we established that since most of the SNe Ia from the H96 flux-limited search were found near maximum, that sample suffered about 0.04 mag of Malmquist bias. On the other hand, some of the R99 SNe Ia were discovered using a galaxy-targeted technique, which therefore is not limited by the SN flux and may be more akin to a volume-limited sample (Li, Filippenko, & Riess 2001). Thus, the addition of the R99 SNe Ia could slightly reduce the overall Malmquist bias of the low-redshift sample. If we were to assume no Malmquist bias for the R99 SNe Ia, and allowing for the fact that they contribute only $\sim 1/4$ the statistical weight of the H96 supernovae, we estimate that the Malmquist bias in the current low-redshift sample is roughly 0.03 mag.

Since Malmquist bias results in the selection of overly-bright supernovae at the limits of a flux-limited survey, and since the flux-limit can be strongly correlated with redshift[30], this bias can

"full-search samples"?

[30] They are 100% correlated for a single field, but this correlation can be diluted by combining fields of different depths.

[This section is begining to sound dangerously vague, perhaps undercutting too much of the current results. I think this whole paragraph could be tightened and simplified.]

result in an apparent distortion of the shape of the Hubble diagram. This may affect estimates of the dark energy equation of state. The selection effects for the current high-redshift supernovae are not sufficiently well-defined to warrant a more detailed modeling of this effect than is presented here. However, for future work, much better control of the selection criteria for SNe Ia at both low- and high-redshift will be required in order to properly estimate the impact of this small, ~~but nearly inescapable,~~ bias.

[SNAP almost completely avoids this bias.]

For the current study, we simply note that since the *differences* in the Malmquist biases of the high- and low-redshift subsets of SN are likely to be *smaller* in this work than in P99, we are less likely to be affected by Malmquist bias. Given the above estimates of 0.03 mag of bias in the low-redshift sample, and 0.02 mag of bias in the high-redshift sample, the *difference* in the biases is only 0.01 mag. To perform a quantitative estimate of the effects of Malmquist bias, we have performed a fit by applying the mean offsets described above to each member of a sample in our primary subset. This fit is plotted in Figure 12b. The H96 supernovae have their magnitudes increased (made dimmer) by 0.04, the P99 supernovae by 0.01, and five of the seven HST supernovae in our primary subset have their magnitudes increased by 0.04. The two HST supernovae (SNe 1998bi, and 2000fr) which were found before maximum light are assumed not to be biased, and the other nine are offset by 0.04, yielding the above estimated 0.03 magnitudes for the sample. A fit with these changed values to the supernova peak magnitudes yields a flat-universe value which is different from our primary fit by $\Omega_{\rm M} = 0.01$, and a value of $\Omega_{\rm M} + \Omega_\Lambda$ which is different by 0.24. The best-fit value of w, when combined with the other cosmological measurements, is 0.02 larger. We adopt these values as our Malmquist bias systematic error.

5.4. K-corrections and Supernova Colors

The generation of the spectral template used for calculating K-corrections is described in § 2.3. The degree to which uncertainties in the K-correction introduce systematic uncertainties into the cosmological parameters depends on whether or not extinction corrections are being individually applied to supernovae. In particular, our K-corrections are most uncertain in the rest-frame U-band range of the supernova spectrum, due to limited published spectrophotometry. As discussed in § 2.2, our primary fits use a spectral template which has a color U-B= 0.4 at the epoch of B-maximum. We have investigated the effects on our cosmology of replacing the spectral template used both for K-corrections and for determining color excesses with a template that has U-B= 0.5 at the epoch of maximum B light.

Figure 12c shows the effect on the fitted cosmology caused by using the different template for calculating K-corrections when individual host-galaxy extinction corrections are not applied. These effects are very mild, indicating that our K-corrections are robust with respect to the intrinsic U-B color of a supernova. Based on the comparison of these fits, we adopt a K-correction systematic uncertainty of 0.17 on $\Omega_{\rm M} + \Omega_\Lambda$ and of 0.01 in w; the systematic uncertainty on the flat-universe value of $\Omega_{\rm M}$ due to this effect is negligible.

Although the effects of a different intrinsic U-B color on the K-corrections are mild, the effects on calculated color excesses are much greater. Figure 12d shows the difference between Fit 6, where host-galaxy extinction corrections have been applied using our standard color-excess values, and a fit where color-excess values have been determined assuming the intrinsic U-B color of a supernova is 0.5 at maximum light. As with other systematics, the primary effect is to move the confidence intervals along their major axis. In this case, the large shift in $\Omega_{\rm M} + \Omega_\Lambda$ is mainly due to the fact that with this bluer reference U-B color, we would believe that all of our $z > 0.7$ supernovae are suffering from an amount of host-galaxy extinction which is greater than that suffered by supernovae at lower redshift. Given that the more distant supernovae are dimmer and thus closer to our detection limits than the moderate redshift supernovae, this scenario is implausible. If anything, one would expect the higher redshift supernovae to be *less* subject to host-galaxy extinction due to selection effects. Nonetheless, a value of U-B= 0.5 at the epoch of B-band maximum is currently ~~unreasonable~~ possible given the U-band information available. Only for those fits where extinction corrections are applied, we have an additional intrinsic U-B systematic error of 0.06 on the flat-universe value of $\Omega_{\rm M}$, and a systematic error of 1.95 on $\Omega_{\rm M} + \Omega_\Lambda$. The systematic uncertainty on w is 0.09. It is likely that

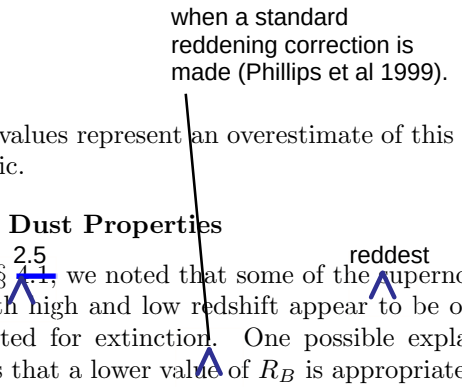

these values represent an overestimate of this systematic.

5.5. Dust Properties

In § 4.1, we noted that some of the supernovae at both high and low redshift appear to be overcorrected for extinction. One possible explanation is that a lower value of R_B is appropriate for SN Ia host galaxies. If we use a value of $R_B = 3.5$ (Phillips *et al.* 1999) rather than the standard value of $R_B = 4.1$ to perform extinction corrections, it slightly changes the best-fit cosmological values for fits where extinction correction are applied (Fit 6); this change is shown in Figure 12e. The flat-universe value of $\Omega_{\rm M}$ changes by 0.02, the best-fit value of $\Omega_{\rm M} + \Omega_\Lambda$ changes by 0.23, and the best-fit value of w when combined with the other cosmological measurements changes by 0.03.

A related source of systematic error is possible evolution in the properties of the host-galaxy dust. Possible evolution in the extinction properties of host-galaxy dust is a source of systematic error in our measurement. To examine the size of the effect, we consider an situation where dust in $z < 0.3$ spiral galaxies have a Cardelli, Clayton, & Mathas (1989) $R_V = 3.1$ law whereas higher-redshift galaxy dust have a ratio of selective-to-total extinction that is half as large, i.e. $R_V = 1.6$. We use the Monte Carlo code described in Kim *et al.* (2003) to study the bias induced when an $R_V = 3.1$ extinction correction is inappropriately applied to all supernovae. We incorporate the redshift and $E(B\text{-}V)$ distributions of the supernovae considered in this paper and an $E(B\text{-}V) < 0.1$ cut is applied. For an input cosmology of $\Omega_{\rm M} = 0.21$ and $\Omega_\Lambda = 0.79$, we find a modest shift in the cosmological parameters to $\Omega_{\rm M} = 0.25$ and $\Omega_\Lambda = 0.77$ without assuming a flat universe.

This bias moves almost exactly along the line $\Omega_M + \Omega_\Lambda = 1$, increasing uncertainty along the thin axis of the error contour. However, the extreme difference in dust properties considered in the Monte Carlo contributes a shift in the cosmological parameters that is less than 1 σ of our quoted statistical error bars. We adopt 0.04 as the "dust evolution" systematic uncertainty on $\Omega_{\rm M}$ in a flat universe for those fits where host-galaxy extinction corrections are applied; this particular systematic is insignificant along the major axis of the confidence ellipses.

The flat-universe value of w, when combined with the 2dFGRS and WMAP results, increases by 0.06 under this simple model of dust evolution. We adopt this as the dust evolution systematic on w for those fits where host-galaxy extinction corrections are applied.

5.6. Gravitational Lensing

Gravitational lensing decreases the modal brightness and causes increased dispersion and positive skewness in the Hubble diagram for high-redshift supernovae. These effects have been discussed in some detail in the literature (Wambsganss *et al.* 1997; Frieman 1997; Holz 1998; Kantowski 1998; Seljak & Holz 1999; Metcalf & Silk 1999; Metcalf 1999; Holz 2001; Wang, Holz, & Munshi 2002; Minty, Heavens, & Hawkins 2002; Amanullah, Mörtsell & Goobar 2003; Dalal *et al.* 2003; Oguri, Suto, & Turner 2003), especially in relation to the P99 and Riess *et al.* (1998) SN datasets. A very conservative assumption of an "empty beam" model in a universe filled with compact objects allowed P99 to demonstrate that gravitational lensing does not alter the case for dark energy. Gravitational lensing may result in a biased determination of the cosmological parameter determination, as discussed in Amanullah, Mörtsell & Goobar (2003). The size of the effect depends on the fraction of compact objects of the total mass density of the universe, $\Omega_{\rm M}$.

The potential bias increases with the redshift of the supernovae in the sample. For example, for the most distant known Type Ia SN, SN1997ff at z=1.7, there is evidence for significant magnification, $\Delta m \sim$ 0.3 (Lewis & Ibata 2001; Mörtsell, Gunnarsson & Goobar 2001; Benitez *et al.* 2002).

As the SN sample considered in this paper does not reach as far, the (de)magnification distortions are expected to be small, in general below 0.05 magnitudes, and less than 1% for the cases considered in P99. To estimate the systematic uncertainties in the cosmological parameters we have used the SNOC package (Goobar *et al.* 2001) to simulate 100 realizations of our data sets assuming a 20% universal fraction of Ω_M in compact objects, i.e. of the same order as the halo fraction deduced for the Milky Way from microlensing along the line of sight to the Large Magellanic Cloud (Alcock *et al.* 2000). The light beams are otherwise assumed to travel through space ran-

domly filled with galaxy halos with mass density with equally divided into SIS and NFW profiles, as described in (Bergström *et al.* 2000). According to our simulations we find that (for a flat universe) the fitted value of Ω_M is systematically shifted by 0.01 on the average, with a statistical dispersion $\sigma_\delta = 0.01$. We adopt 0.01 as our gravitational lensing systematic error in the flat-universe value of $\Omega_{\rm M}$. The effect on $\Omega_{\rm M} + \Omega_\Lambda$ is very small compared to other systematics, biasing the sum by only 0.04.

The simulated offsets due to gravitational lensing, when combined with CMB and galaxy redshift distortion measurements, increase the value of w by 0.05; we adopt this as a gravitational lensing systematic on w.

5.7. Supernova Population Drift

In P99 we discussed in detail whether the high-redshift SNe Ia could have systematically different properties than low-redshift SNe Ia, and in particular, whether intrinsic differences might remain after correction for stretch. One might imagine this to occur if the range of the physical parameters controlling SN Ia brightnesses have little overlap between low- and high-redshift such that corrections applied to low-redshift are inappropriate or incomplete for high-redshift SNe Ia. Since P99, considerable additional work has been done to address this issue.

In addition to comparisons of stretch range, as well as spectral Perlmutter *et al.* (1998) and lightcurve (Goldhaber *et al.* 2001) features, several tests performed directly with the P99 high-redshift SNe Ia have shown excellent consistency with low-redshift SNe Ia. Most recently, in Sullivan *et al.* (2003) we have presented results on the Hubble diagram of distant Type Ia supernovae from P99 that have been morphologically-typed with HST. We found no difference in the cosmological results from their morphologically-segregated subsamples. In particular, E/S0 galaxies — for which one expects the tightest possible correlation between progenitor mass and redshift — not only agree with the cosmological fits using only spiral galaxies, but by themselves confirm the results of P99. This is strong evidence that, while age or metallicity could in principle affect the brightnesses of SNe Ia, stretch correction eliminates these differences. Likewise, the lightcurve rise-time — suggested as an indicator of the energetics of the SN explosion (see Nugent *et al.* 1995; Hoeflich, Wheeler, & Thielemann 1998) — while initially suggested to be different between high- and low-redshift SNe Ia (Riess *et al.* 1999b), has been demonstrated to agree very well (Aldering, Knop, & Nugent 2000, within 1.8 ± 1.2 days).

On the theoretical side, the SN formation models of Kobayashi *et al.* (1998); Nomoto, Nakamura, & Kobayashi (1999) suggest that the progenitor binary system must have [Fe/H]$>$ 1 in order to produce a SN Ia. This would impose a lower limit to the metallicities of all SNe Ia, and thus limit the extent of any metallicity-induced brightness differences between high- and low-redshift SNe Ia. On the empirical side, the lack of a gradient in the intrinsic luminosities of SNe Ia with galactocentric distance, coupled with the fact that metallicity gradients are common in spiral galaxies (Henry & Worthey 1999), lead Ivanov, Hamuy, & Pinto (2000) to suggest that metallicity is not a key parameter in controlling SNe Ia brightnesses at optical wavelengths— though note that Lentz *et al.* (2000) show how it can affect the ultraviolet. In addition, Hamuy *et al.* (2000, 2001) find that lightcurve width is not dependent on host-galaxy metallicity.

Alternatively, population age effects, including pre-explosion cooling undergone by the progenitor white dwarf and other effects linked to the mass of the primary exploding white dwarf have been suggested (for a review, see Ruiz-Lapuente 2003). As the local sample of SNe Ia represents populations of all ages and metallicities, both effects can be studied locally. Several low-redshift studies have presented data suggesting that SNe Ia intrinsic luminosities (i.e., those prior to stretch correction) may correlate with host-galaxy environment (Hamuy *et al.* 1996b; Branch, Romanishin, & Baron 1996; Wang, Hoeflich, & Wheeler 1997; Hamuy *et al.* 2000; Ivanov, Hamuy, & Pinto 2000; Howell 2001; Wang *et al.* 2003, R99). These findings are actually encouraging, since unlike stretch itself, there is some hope that host-galaxy environment variations can be translated into the types of physical parameters such as age and metallicity which can help in relating any drifts in the SNe Ia population to galaxy evolution.

More importantly for cosmology, R99 used their sample of 22 local SNe Ia to demonstrate that any

[Should we say anything about why this line doesn't look like a great fit -- a zero slope looks almost as good, doesn't it? Are the reddened SNe distorting something in this graph?]

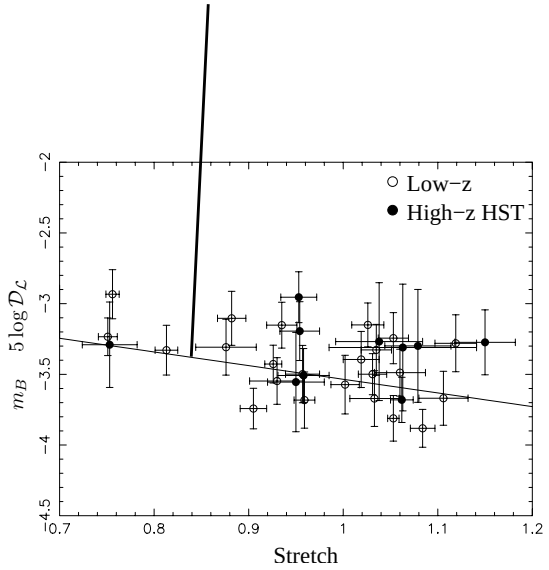

Fig. 13.— Stretch-luminosity relationship for low-redshift SNe (open circles) and high-redshift HST SNe (filled circles). Each point is the measured m_B for that supernova, minus $\mathcal{D}_\mathcal{L}$, the "Hubble-constant-free luminosity distance" (see § 2.4), plotted against the stretch of that SN. The line drawn represents the best-fit values of α and $\mathcal{M}$ from Fit 6, the fit to all Subset 1 supernovae with host-galaxy extinction corrections applied. Note in particular that our HST SNe Ia all have low-redshift counterparts.

brightness variations between SNe Ia in different host-galaxy environments disappear after correction for lightcurve width. We have quantified this agreement using a larger local sample of supernovae, 14 of which have E/S0 hosts and 27 of which have spiral hosts (Wang *et al.* 2003). We find that after lightcurve-width correction there can be less than a 0.01 ± 0.05 mag offset between SNe Ia in local spirals and ellipticals. This indicates that lightcurve width is able to correct for age or other differences.

Finally, Wang *et al.* (2003) demonstrate a new method, *CMAGIC*, which is able to standardize the vast majority of local SNe Ia to within 0.08 mag (in contrast to $\sim$ 0.11 mag which lightcurve width corrections can attain (Phillips *et al.* 1999)). This imposes even more severe limits on the fraction of SNe Ia generated by any alternate progenitor scenario, or requires that variations in the progenitor properties have little effect on whether the resulting SN can be standardized.

The data from the new SNe Ia presented here do offer one new test for consistency between low- and high-redshift SNe Ia. The quality of our HST data provides measurements of the SN peak magnitudes and lightcurve widths rivaling those for nearby SNe Ia. This allows a direct comparison between the stretch-luminosity relations at low- and high-redshifts. This comparison is shown in Figure 13. This plot shows that the HST high-redshift supernovae are found at similar stretches as the low-redshift supernovae, and are consistent with the same stretch-luminosity relationship.

5.8. Possible Additional Sources of Systematic Uncertainties

Other potential sources of systematic uncertainties have been suggested. E.g., Aguirre (1999a,b); Aguirre & Zoltan (2000) argued that the presence of "grey" dust, i.e. a homogeneous intergalactic component with weak differential extinction properties over the rest-frame optical wavelength regime could not be ruled out by the P99 data. Since then, the Hubble diagram of Type Ia supernovae beyond $z = 1$ (Riess *et al.* 2001) was claimed to rule out the "grey" dust scenario as a non-cosmological alternative explanation to the dimming of high-redshift supernovae; however, there remain some outstanding issues with this interpretation (e.g., Goobar, Bergström, & Mörtsell 2002; Blakeslee *et al.* 2003). A direct test for extinction over a wide wavelength range, rest-frame B-I, have been performed by Riess *et al.* (2000) on a single supernova, SN 1999Q, which showed no grey dust signature; however, see Nobili *et al.* (2003). Although the situation remains inconclusive, there is no direct evidence that "grey" dust is a dominant source of uncertainties. It remains an important issue to be addressed by future data sets including near-infrared observations.

More recently, the possibility of axion-photon oscillations making high-redshift supernovae to appear dimmer was suggested by Csaki, Kaloper, & Terning (2002). This attenuation would be wavelength dependent, and thus be explored with spectroscopic studies of high-shift sources (Mörtsell, Bergstrom, & Goobar 2002). Preliminary studies of QSO spectra between $z = 0.15$ and $z = 5.3$ set a very conservative upper limit on the possible dimming of z$\sim$0.8 supernovae to 0.2 magnitudes (Mörtsell & Goobar 2003)

For the current data sample, the above mentioned sources of systematic uncertainties appear to be subdominant in the total error budget.

5.9. Total Identified Systematic Uncertainty

The identified systematic errors are summarized in Table 9. Adding together these errors in quadrature, we obtain a total systematic error of 0.04 on the flat-universe value of Ω_M (along approximately the minor axis of the confidence ellipses shown in Ω_M vs. Ω_Λ plots); this is smaller than but approaching our statistical uncertainty of 0.06. The total systematic uncertainty on $\Omega_M + \Omega_\Lambda$ is 0.95 (along approximately the major axis of the confidence ellipses). Finally, for the low-extinction subset, we have a systematic uncertainty on constant w of 0.08, less than our high-side systematic uncertainty of 0.14.

For fits with host-galaxy extinction corrections applied, we have to consider the additional systematic effects of an uncertainty in the intrinsic value of U-B on determined color excesses, and of dust properties. In this case, we have a total systematic error of 0.09 on the flat-universe value of Ω_M or Ω_Λ, and a total systematic error of 2.2 on $\Omega_M + \Omega_\Lambda$; as discussed in § 5.4, this is likely to be an overestimate of the true systematic error. The total systematic uncertainty on constant w for the extinction-corrected full primary sample is 0.14.

6. Summary and Conclusions

1. We present a new, independent set of eleven high-redshift supernovae ($z = 0.36$–0.86). These supernovae have very high-quality photometry measured with WFPC2 on the HST. The higher quality lightcurve measurements have small enough errors on each $E(B\text{-}V)$ measurement to allow an unbiased correction of host-galaxy reddening. We have performed improved color and K-corrections, necessary to combine WFPC2 photometric filters with ground-based photometric filters.

2. The cosmological fits to Ω_M and Ω_Λ are consistent with the SCP's previous results (P99), providing strong evidence for a cosmological constant. This is a significant confirmation of the results of P99 and Riess *et al.* (1998), and represents a completely new set of high-redshift supernovae yielding the same results as the earlier supernova work. Moreover, these results are consistent with a number of other cosmological measurements, and together current observation cosmology is pointing towards a consensus $\Omega_M \sim 1/4$, $\Omega_\Lambda \sim 3/4$ Universe.

3. Most identified systematic errors on Ω_M and Ω_Λ affect the cosmological results primarily by moving them along the direction where they are most uncertain, that is, along the major axis of the confidence ellipses. ~~In this~~ direction, our total identified systematic error is 0.95 on $\Omega_M + \Omega_\Lambda$ for the low-extinction primary subset, and 2.2 on the extinction-corrected full primary subset. Given the large size of these systematics in this direction, any conclusions drawn from the positions of supernova confidence ellipses along this direction should be approached with caution.

   Systematics are much smaller along the small (approximately Ω_M Ω_Λ) axis of the confidence regions, and may be described by giving the systematic error on Ω_M or Ω_Λ alone in the flat-universe case. Our total identified systematic error for the low-extinction sample analysis is 0.04 on the flat-universe value of Ω_M or Ω_Λ. When host-galaxy extinction corrections are applied, a conservative estimate of the total identified systematic error is 0.09.

4. Under the assumption of a flat universe with vacuum energy (constant $w = -1$), we find a value of $\Omega_M = 0.22 \pm 0.06$ (statistical) ± 0.04 (identified systematic), indicating a cosmologcial constant of $\Omega_\Lambda = 0.78 \pm 0.06$ (statistical) ± 0.04 (identified systematic). This result is robust to host-galaxy exctinction, and a fit with full, unbiased, individual extinction corrections applied yields a flat-universe cosmological constant of $\Omega_\Lambda = 0.72^{+0.10}_{0.12}$ (statistical) ± 0.09 (identified systematic). Our best confidence regions for Ω_M versus Ω_Λ are shown in Figure 7.

5. When combined with the 2dFGRS galaxy redshift distortion measurement and WMAP

In the more uncertain, major axis

[Would this really be a "consensus" today, or would other measurements tend towards higher Omega_m, lower Omega_lambda?]

Switch the order of these two boxes.

Table 9: Identified Systematic Errors

Source of Uncertainty	Systematic Uncertainty On: Flat-Universe $\Omega_{\rm M}$or Ω_Λ[a]	$\Omega_{\rm M}+\Omega_\Lambda$	constant w[b]	Notes
Fit method	0.03 (0.5σ)	0.80	0.02	
Type contamination	0.03 (0.5σ)	0.42	0.06	
Malmquist Bias	0.01 (0.2σ)	0.24	0.02	
Intrinsic U-B: K-corrections	0.00 (0.0σ)	0.17	0.01	*c*
Gravitational Lensing	0.01 (0.2σ)	0.04	0.05	
Systematic with host-galaxy extinction corrections:				
Intrinsic U-B: color excess	0.06 (0.6σ)	1.95	0.09	*d*
Extinction Slope	0.02 (0.2σ)	0.23	0.03	*d*
Dust Evolution	0.04 (0.4σ)	0.02	0.06	*d*

a: Each systematic is given as an offset from the flat-universe value of $\Omega_{\rm M}$, and in terms of the smaller side of the statistical error bar (0.06 for Fit 3 to the low-extinction subset, 0.10 for Fit 6 to the full primary subset).
b: This is the offset on the maximum-likelihood value of w when the the low-extinction subset fits (Fit 3) is combined with the 2dFGRS and WMAP measurements of $\Omega_{\rm M}$ and w.
c: Only used where host-galaxy extinction corrections are not applied; when $E(B\text{-}V)$ corrections are applied, host-galaxy extinction enters in as a statistical error.
d: Only used where host-galaxy extinction corrections are applied.

This extra line-space should be after the "Grav Lensing" line, not before.

CMB data, we find a value for the dark energy equation of state parameter $w = 1.06^{+0.14}_{0.21}$, under the assumptions that the Universe is spatially flat and that w is constant in time. The identified systematic uncertainty on w is 0.08. The current confidence regions on the flat-universe values of $\Omega_{\rm M}$ and w are shown in Figure 11. The supernovae data are consistent with a low-mass Universe dominated by vacuum energy ($w = -1$), but they are also consistent with a wide range of constant or time-varying dark energy models.

The authors wish to thank our HST program coordinator, Doug Van Orsow for his help in the planning, scheduling, and execution of the observations presented herein. Support for this work was provided by NASA through grants HST-GO-07336.01-A and HST-GO-08346.01-A from the Space Telescope Science Institute, which is operated by the Association of Universities for Research in Astronomy, Inc., under NASA contract NAS 5-26555. The authors are indebted to Drs. Malcolm Smith and Patrick Hall for trading several crucial hours of observing time at the CTIO 4-m, which played a key role in our SN search in March 1998. The authors acknowledge the tremendous help of the night assistants and support staff at the many telescopes from which data for this paper were obtained; we are particularly grateful to the CTIO staff for crucial support during our key search nights, and to Di Harmer and Paul Smith of the WIYN Queue. We thank Gary Bernstein and Tony Tyson for developing and supporting the Big Throughput Camera at the CTIO 4-m. This wide-field camera was important in the discovery of most of the high-redshift supernovae presented in this paper, and enabled the high discovery rate needed to guarantee supernovae for follow-up with HST. We also wish to acknowledge NOAO for providing and supporting the astronomical data reduction package IRAF. The authors wish to recognize and acknowledge the very significant cultural role and reverence that the summit of Mauna Kea has always had within the indigenous Hawaiian community. We are most fortunate to have the opportunity to conduct observations from this mountain. This work was supported in part by the Director, Office of Science, Office of High Energy and Nucler Physics, of the U.S. Department of Energy under Contract

[For Saul and Greg (anyone?) to do?: It would really help polish this paper if we can come up with one more paragraph to round out this conclusion section, perhaps tying what we have found into some of the larger questions and the larger context.]

No. DE-AC03-76SF000098, by the Center for Particle Astrophysics, an NSF Science and Technology Center operated by the University of California, Berkeley, under Cooperative Agreement No. AST-91-20005. P. E. Nugent acknowledges support from a NASA LTSA grant. Finally, the authors are grateful to Eric Linder for the use of his growth-parameter solver, and to Ramon Miguel for assistance with gravitational lensing calculations.